Source Apportionment of $PM_{2.5}$ in Montréal, Canada and Health Risk Assessment for Potentially Toxic Elements

Nansi Fakhri[1,2], Robin Stevens[2,3], Arnold Downey[2], Konstantina Oikonomou[4], Jean Sciare[4], Charbel Afif*[1,4], Patrick L. Hayes*[2]

[1] EMMA Research Group, Centre d'Analyses et de Recherche, Faculty of Sciences, Université Saint-Joseph, Beirut, Lebanon
[2] Department of Chemistry, Faculty of Arts and Sciences, Université de Montréal, Montréal, Québec, Canada
[3] School of Public Health, Université de Montréal, Montréal, Québec, Canada
[4] Climate and Atmosphere Research Center (CARE-C), The Cyprus Institute, Nicosia, Cyprus

Correspondence to: Patrick L. Hayes (patrick.hayes@umontreal.ca); Charbel Afif (charbel.afif@usj.edu.lb)

Abstract. Source apportionment of $PM_{2.5}$ was performed using positive matrix factorization (PMF) based on detailed chemical composition data from 24-h filter samples collected over a 3-months period (August-November 2020) at an urban site in Montréal, a Canadian city with a population of approximately 4 million people. This source apportionment study, which examined the main contributing sources to $PM_{2.5}$ using a larger suite of organic molecular markers than other Canadian studies, is the first of its sort in Canada. A focus of this study was on quantifying previously unresolved sources of $PM_{2.5}$ through the inclusion in the PMF analysis of additional organic molecular markers beyond those measured typically by the Canadian government's National Air Pollution Surveillance Program (NAPS). ~~The organic species included in the PMF model were namely, n-alkanes, hopane, fatty acids, dicarboxylic acids, and biogenic secondary organic aerosols (SOA) tracers.~~ The organic species included in the PMF model were comprised of six n-alkanes, two fatty acids, one dicarboxylic acid, two biogenic secondary organic aerosols (SOA) tracers and hopane. Secondary inorganic aerosols (SIA) and SOA were the dominant components and constituted 39% of the measured $PM_{2.5}$ mass while the local primary anthropogenic sources, namely traffic exhaust, road dust, industrial, and cooking emissions contributed 23%. The chemical transport model GEOS-Chem revealed that ammonium sulfate concentrations in Montréal are strongly influenced by both local sources in Québec and transboundary input from the United States, with the transboundary input exceeding the local emissions for SOA. Co and Cr(VI) presented an elevated cancer risk, highlighting that more attention should be given to these trace metals, which were associated with industrial emissions by the PMF analysis. Furthermore, the results showed that industrial emissions were minor contributors to the total $PM_{2.5}$ mass concentration, but were the largest contributors to Co and Cr(VI) concentrations. Thus, the health hazards associated with this source cannot be entirely established by the $PM_{2.5}$ mass concentration alone. This study highlights that, when evaluating air quality in Montréal and other urban regions, the prioritization of sources for mitigations strategies will diverge if one considers total $PM_{2.5}$ mass concentration or the concentration of individual particulate-bound contaminants. Furthermore, the large transboundary contribution from the United States to total $PM_{2.5}$ levels suggests that future municipal, provincial and federal monitoring and regulations would be more effective if they focus on specific high-risk contaminants (e.g., Co and Cr(VI) rather than total $PM_{2.5}$.

1 Introduction

Outdoor air pollution is a serious threat to human health and is responsible for over 4 million premature deaths worldwide annually (Nansai et al., 2021). Among the various air pollutants, particulate matter (PM) is one of the most problematic and has been classified within Group 1 "carcinogenic to humans" by the International Agency for Research on Cancer (IARC). Particle size is a critical parameter for assessing health impacts, and PM with an aerodynamic diameter less than 2.5 µm ($PM_{2.5}$) represents a greater threat to health than coarser particles as these fine particles can penetrate deeply into the respiratory tract and induce adverse health effects such as respiratory and cardiovascular diseases (Lelieveld et al., 2019).

Outdoor air pollution continues to have serious health consequences in Canada (EAR, 2019; Jeong et al., 2011; Bari & Kindzierski, 2016). The government of Canada estimates that approximately 15,300 premature deaths per year are linked to air pollution (Health Canada, 2021). Montréal, a Canadian city in the province of Québec, is the largest city in the province and the second largest in Canada with a population of approximately 4 million people. The city maintains a network of 14 air quality monitoring stations that continuously measure the concentrations of major pollutants (e.g., PM, ozone, sulfur dioxide (SO_2), nitrogen oxides (NO_X), ozone etc.). These municipal monitoring stations also belongs to Environment and Climate Change Canada's National Air Pollution Surveillance (NAPS) program which is the principal source of ambient air quality data in Canada (EAR, 2020) and provides also speciated PM composition measurements via off-line analyses at a limited number of sites. The resulting data enable a portrait to be drawn of the evolution of pollutant concentrations in Montréal over the years. The concentrations of $PM_{2.5}$ in Montréal's ambient air have been decreasing since 2011. The 3-year average concentration of $PM_{2.5}$ decreased from 9.7 µg/m^3 (2011-2013) to 7.3 µg/m^3 (2018-2020) (EAR, 2017; 2018; 2019; 2020). However, in September 2021, WHO released revised global air quality guidelines with a recommended $PM_{2.5}$ concentration of 5 µg/m^3, meaning that the $PM_{2.5}$ concentrations in Montréal exceed WHO recommendations (WHO, 2021). Thus, it is important to continue to improve air quality in the city.

To effectively reduce PM emissions in the metropolitan area and design effective local PM control strategies, it is necessary to have a better understanding of the dominant emission sources and associated health risk. Over the years several efforts have been made to improve the knowledge about the sources of atmospheric particles in Canada using the receptor-based source apportionment model ~~positive~~ Positive ~~matrix~~ Matrix ~~factorization~~ Factorization (PMF) and NAPS $PM_{2.5}$ chemical speciation datasets as inputs (Bari & Kindzierski, 2016; Dabek-Zlotorzynska et al., 2011; Jeong et al., 2011; Celo et al., 2021). In Québec, there are six NAPS sites that provide speciated $PM_{2.5}$ measurements, three of which are in the Montréal area namely Châteauneuf (NAPS ID: S50124), Molson (NAPS ID: S50134) and Rivière des Prairies (NAPS ID: S50129). However, samples are collected once every 3 or 6 days, and operating on this sampling frequency does not allow reliable quantification of the concentration distribution's extremes because this sampling schedule may exclude days of very high or low concentrations from a given source. Another limitation is the lack of data on organic compounds, which can be valuable tracers for certain $PM_{2.5}$ sources (Fadel et al., 2021, Fakhri et al., 2023). To date, investigations of PM concentrations and

chemical composition from NAPS sites in Canada have generally focused on determining the elemental (EC) and organic carbon (OC) concentrations as well as the elemental and ionic content of PM.

In this work, $PM_{2.5}$ chemical composition and emission sources as well as potential human health risk associated with trace elements in ~~the~~ $PM_{2.5}$ are investigated for an urban site in Montréal over a 3-month period (August-November). In addition to water-soluble ions, elements, EC, and OC, the measurements of $PM_{2.5}$ composition included a large suite of organic molecular markers. This study uses these measurements to explore qualitatively potential sources (e.g., via correlations of elements) before proceeding to a more quantitative approach to source apportionment using PMF. Source apportionment of $PM_{2.5}$ was performed using simultaneously organic and inorganic species in the PMF model. The aim of this work is to investigate previously unresolved PM sources in Montréal, such as primary and secondary biogenic and anthropogenic sources by using some selected organic markers, namely n-alkanes, hopane, fatty acids, dicarboxylic acids, and biogenic secondary organic aerosol tracers in the PMF model. To our knowledge, this study represents the first time that such extensive composition measurements were included in a source apportionment study in Montréal. Furthermore, the GEOS-Chem chemical transport model was used to evaluate local and long-range contributions to the most significant PM components, providing more information on the origin of PM. Lastly, a health risk assessment model was used to determine the associated risk of the elemental components from the sources identified using the PMF model.

2 Method

2.1 $PM_{2.5}$ Sampling

Sampling was conducted at an urban site in Montréal from 13 August to 11 November 2020. The sampling site, labeled as MTL, was located on the rooftop of Campus MIL (12 m above ground level) at the University of Montréal (45°31′~~23~~21" N, 73°37′~~10~~14" W) in the neighbourhood of Outremont. The site is characterized by a high density of residential and commercial premises.

A total of 80 $PM_{2.5}$ filter samples (150 mm quartz-fiber filters, PALL) were collected with a 24 h resolution using a high-volume sampler (CAV-A/MSb, MCV S.A., Spain) operating at 30 m^3/h. Filters were baked at 550 °C for 12 h before sampling to eliminate the organic impurities and kept at -20 °C until sampling. Collected filters were also stored at -20 °C until analysis. Field blank samples were collected by loading filters into the sampler but without operating the sampler's pump. A total number of 8 field blank samples were also analyzed with the same techniques as the sample filters. The concentrations of the species in the $PM_{2.5}$ samples were corrected by subtracting the average field blank values. Additional QA/QC procedures were applied on the different analysis techniques/protocols used (e.g., determination of detection limits and recovery, as well as validation using certified reference material) (Fakhri et al., 2023). $PM_{2.5}$ mass concentration was determined by weighing the filters before and after sampling using a VWR microbalance with a 1 µg readability (Abdallah et al., 2018, Fadel et al., 2022b).

2.2 Chemical analysis

The chemical analyses are detailed in Fakhri et al. (2023) and will only be briefly presented here. Elemental carbon (EC) and organic carbon (OC) were analyzed using the thermo-optical transmission method on a Sunset Laboratory analyzer following the EUSAAR2 (European Supersites for Atmospheric Aerosol Research) protocol (Cavalli et al., 2010).

Major (Al, Fe, K, Mg, Na) and trace (Zn, Ni, Sr, Cu, Ti, Co, Cr, V, Mn, Cd, Mo, Sb, Pb) metals and metalloids were analyzed using an inductively coupled plasma mass spectrometer (ICP-MS) (PerkinElmer, NexION, 300x). In brief, a punch (18 mm^2) was taken from the quartz filters and digested in a mixture of ultrapure HNO_3 (4 mL of 67-70% (w/w), Baker ARISTAR ULTRA supplied by VWR International) and HCl (1 mL of 35-38% (w/w), Trace Metal Grade, Fischer Chemical) in a Microwave Reaction System (CEM, Mars-Xpress, MARS 230/60). The oven program was set to an initial temperature ramp reaching 180 °C in 5.5 min with a subsequent holding period of 9.5 min. Matrix-matched ICP-MS calibration standards were prepared using IV-ICPMS-71a (Inorganic Ventures) and quality control standards were prepared using QCS-27 (High-Purity Standards). Two external calibration methods were used for sample analysis: one for trace metals and metalloids where the calibration range was between 0.05 and 10 µg/L, and the other for the analysis of major metals where the calibration range was between 3 and 500 µg/L. The calibration curves showed good linearity with R^2 greater than 0.999. An internal standard solution comprised of Sc, Y, In, and Bi was analyzed along with the samples, with recovery ranging from 90 – 130%. The analytical procedure was validated by considering a certified reference material NIST-SRM 1648a (Urban particulate matter, National Institute of Standards and Technology, United States of America). Data for a given metal were accepted as quantitative if NIST SRM 1648 recovery was 80 – 110%.

Soluble anions and cations were analyzed by ionic chromatography after extracting a punch (20 mm) of each quartz filter by ultrasonic agitation in 6 mL of MilliQ water (Elga Veolia Purelab Chorus 1, 18.2 MΩ at 25 °C) for 45 min, by means of a Dionex ICS 5000^+ instrument. For anion analysis, a Dionex IonPac AS11-HC anion column (2×250 mm), a Dionex IonPac AG11-HC (2×50 mm) pre-column and a Dionex AERS 500 suppressor were used. Thermo Scientific Dionex KOH with a gradient of 1-45 mM was used as the eluent in the anion analysis with a flowrate of 0.5 mL/min. For cation analysis, a Dionex IonPac CS12 cation column (2×250 mm), a Dionex IonPac CG12 (2×50 mm) pre-column and a Dionex CSRS 300 4 mm suppressor were used during the cation analysis. Thermo Scientific Dionex 12 mM methanesulfonic acid with a flowrate of 0.3 mL/min was used as eluent in the cation analysis.

Sugar alcohols were analyzed by ion chromatography with pulsed amperometric detection (IC-PAD) by means of a Dionex ICS 5000^+ instrument using a Dionex CarboPac MA1 column (4×250 mm) and a Dionex CarboPac MA1 (4×50 mm) pre-column. Thermo Scientific Dionex 0.35 M NaOH with a flowrate of 0.6 mL/min was used as eluent in the sugar analysis.

The method used for the organic compounds analysis was described elsewhere (Fadel et al., 2021; Fakhri et al., 2023; El Haddad et al., 2011). Briefly, a punch of the sample filter (73 cm^2) was spiked with two internal standards (D50-tetracosane and D6-cholesterol obtained from Sigma Aldrich) followed by an extraction using an accelerated pressurized solvent extraction device at 100 °C and 100 bar~~s~~ (ASE, Dionex 350) and an acetone/dichloromethane mixture (1/1, v/v). After

extraction, samples were concentrated to a volume of 200 µL using a constant gentle flow of nitrogen gas. 50 µL of the extracts was then derivatized with the addition of 50 µL of N,O-bis(trimethylsilyl)- trifluoroacetamide (BSTFA) (99%, Sigma Aldrich) with 10 µL of pyridine (catalyst) (99%, Sigma Aldrich) at 70 °C for 2 h. Aliquots of 2 µL of the derivatized extracts were immediately analyzed using a GC-MS in split mode. In addition, aliquots of 2 µL of the non-derivatized fraction were also analyzed using the GC-MS in split mode. The gas chromatograph (Agilent 6890N) was equipped with a HP-5MS UI fused silica capillary column (5%-phenyl, 95%-methylpolysiloxane, 0.25 µm film thickness, and 30 m × 0.25 mm) and interfaced to an ion trap MS with an external electron ionization (EI) source (200 °C, 70 eV). Full scan mode was used in the mass range of 50-550 m/z.

2.3 ~~Enrichment factor~~Chemical mass closure

The term "chemical mass closure" refers to the reconstruction of the measured weighed mass using just the chemical composition. It is done by comparing the combined masses of the chemical species to the gravimetric particulate matter mass (m_{grav}), wherein the reconstructed $PM_{2.5}$ mass (m_{chem}) is defined as the sum of organic matter (OM), EC, crustal matter, sea salt, secondary inorganic aerosol (SIA), and other elements that are not taken into account as minerals (Chow et al., 2015).

A chemical mass closure study was performed using the chemical composition measurements to estimate the contributions of the different components to the total $PM_{2.5}$ mass concentration following the method reported by Fakhri et al. (2023). Briefly, the contribution of sea salt is calculated by summing the six major ions (Sciare et al., 2005):

$$[\text{Sea salt}] = [Na^+] + [Cl^-] + [ss - Mg^{2+}] + [ss - K^+] + [ss - Ca^{2+}] + [ss - SO_4^{2-}] \quad (Eq.\ 1)$$

Ionic constituents such as K^+, Ca^{2+}, Mg^{2+} and SO_4^{2-} are derived from both marine and non-marine sources. Therefore, it is necessary to discriminate sea salt (ss) from non-sea salt (nss) contributions. Assuming that all sodium ions are of marine origin, the sea salt contribution can be calculated based on sea water composition as shown in Eqs. 2 - 5 (Genga et al., 2017; Sciare et al., 2005). Furthermore, non-sea salt potassium, calcium, magnesium and sulfate (nss-K^+, nss-Ca^{2+}, nss-Mg^{2+} and nss-SO_4^{2-}) are calculated by subtracting the sea-salt fraction (ss-K^+, ss-Ca^{2+}, ss-Mg^{2+} and ss-SO_4^{2-}, respectively) from the total concentration of the ions (K^+, $Ca2^+$, Mg^{2+} and SO_4^{2-}, respectively).

$$[ss - SO_4^{2-}] = 0.252 \times [Na^+] \quad (Eq.\ 2)$$

$$[ss - Ca^{2+}] = 0.038 \times [Na^+] \quad (Eq.\ 3)$$

$$[ss - K^+] = 0.036 \times [Na^+] \quad (Eq.\ 4)$$

$$[ss - Mg^{2+}] = 0.119 \times [Na^+] \quad (Eq.\ 5)$$

In addition, secondary inorganic aerosol (SIA) is represented by the sum of nss-SO_4^{2-}, NH_4^+ and NO_3^-. To take bound water into account a hydration multiplication factor of 1.29 was applied to convert the dry inorganic concentrations (SIA and sea salt) into hydrated species (Sciare et al., 2005; Genga et al., 2017).

The contribution of crustal matter (CM) (Eq. 6) was estimated by summing the concentrations of aluminum, silicon, calcium, iron, and titanium in their oxide forms (Huang et al., 2014). The coefficients in front of the elements correspond to the additional mass due to oxygen in the minerals. Silicon was not measured in this study and was indirectly determined by multiplying the measured aluminum concentration by a factor of 3.41 (Esmaeilirad et al., 2020). This factor is obtained from the ratio of Si and Al in the Earth's crust following Mason and Moore (1982).

$$[CM] = 2.2\,[Al] + 2.49\,[Si] + 1.63\,[Ca] + 2.42\,[Fe] + 1.94\,[Ti] \qquad (Eq.\,6)$$

To find the optimal CF to calculate OM from OC, the factor was varied from 1.2 to 2.1. The Pearson correlation (R) calculated between the reconstructed $PM_{2.5}$ and the measured mass did not change significantly (0.978-0.979), but the highest correlation and the slope closest to 1 was obtained with CF=1.6. The results of chemical mass closure study are shown in Fig. S5.

~~The enrichment factor (EF) was calculated to determine whether a certain element in $PM_{2.5}$ may have a significant anthropogenic source. EF (Eq. 1) is defined as the ratio of the considered element concentration (C_X) to the reference element concentration Al (C_{Al}) in $PM_{2.5}$ divided by the same ratio for crustal material retrieved from the upper crust (Mason & Moore, 1982). An EF value close to 1 indicates an element originates from crustal materials while an EF higher than 10 indicates a strong anthropogenic source (Esmaeilirad et al., 2020).~~

~~$$EF = \left(\frac{C_X}{C_{Al}}\right)_{air} / \left(\frac{C_X}{C_{Al}}\right)_{crust} \qquad (Eq.\,1)$$~~

2.4 Health risk assessment

The United States Environmental Protection Agency (USEPA) recommends using a health risk assessment model to determine the health risks from airborne elements. For each of the three exposure pathways, namely inhalation, ingestion, and dermal contact, the carcinogenic and non-carcinogenic health risks were evaluated for children and adults using the measurements taken at the MTL site. This study analyzes the non-carcinogenic risks of Al, Fe, Cu, Zn, Sb, Co, Cr(VI), Ni, V, Cd, Pb and Mn as well as the carcinogenic risk of Cr(VI), Co, Ni, V, Cd and Pb. The average daily dose (ADD in mg/kg per day) for children (0-17 years) and adults (18-70 years) for the three exposure pathways and the exposure concentration

through inhalation ($EC_{inhalation}$ in mg/m^3) were calculated following Eqs ~~2-5~~ 7-10 (Fadel et al., 2022a, 2022b; Roy et al., 2019). Each of the parameters used in the various formulas are listed in **Table 1** and were retrieved from USEPA reports (USEPA 2004, 2011). Moreover, since chromium toxicity is attributed to its hexavalent state, Cr(VI) concentration was determined as one-seventh of total Cr (Dahmardeh Behrooz et al., 2021; Hao et al., 2020, Fadel et al., 2022b).

$$ADD_{ingestion} = \frac{C \times IngR \times EXP \times ED \times CF}{BW \times AT} \quad \text{(Eq. ~~2~~7)}$$

$$ADD_{dermal} = \frac{C \times SA \times AF \times ABS \times EXP \times ED \times CF}{BW \times AT} \quad \text{(Eq. ~~3~~8)}$$

$$ADD_{inhalation} = \frac{C \times InhR \times EXP \times ED \times CF}{BW \times AT} \quad \text{(Eq. ~~4~~9)}$$

$$EC_{inhalation} = \frac{C \times EXP \times ED \times ET \times CF}{AT \times 24} \quad \text{(Eq. ~~5~~10)}$$

Table 1: Exposure parameters for children and adults.

Exposure parameters		**Unit**	**Adults**	**Children**
Concentration of metal in $PM_{2.5}$	C	ng/m^3 (inhalation) and mg/kg (ingestion and dermal)		
Ingestion rate	IngR	mg/day	50	100
Inhalation rate	InhR	m^3 per day	15.6	12.3
Exposure frequency	EXP	days/year	350	350
Exposure duration	ED	years	52	17
Conversion factor	CF	kg/mg	10^{-6}	10^{-6}
Body weight	BW	kg	70	37
Exposed skin area	SA	cm^2	5700	2800
Adherence factor	AF	mg/cm^2	0.07	0.2
Exposure time	ET	h/day	8	8
Dermal adsorption factor	ABS	-	0.001 for Cd 0.01 for other metals	
Averaging time	AT	days	Non-carcinogens: AT=ED × 365 (days) Carcinogens: AT=70 years × 365	

The hazard quotient (HQ), which is determined by dividing the ADD from each exposure pathway by a specified reference dose (R_fD) (mg/kg per day) for the same exposure route, can be used to measure the non-carcinogenic health risk effects from metals as presented in Eq. ~~6~~ 11 (Fadel et al., 2022a, 2022b; Hao et al., 2020). The non-cancer risk refers to the likelihood of developing health issues other than cancer as a result of exposure to chemical pollutants such as asthma, nervous system disorders, cardiovascular and respiratory disorders (Fadel et al., 2022a).

To assess the overall potential for non-carcinogenic consequences produced by multi-element exposure for one exposure pathway, the hazard index (HI_i) was calculated as the sum of the HQ_{ij} (i is the exposure pathway which is either inhalation, ingestion, or dermal contact, and j is the targeted compound) (Eq. ~~7~~12). HI_{total} represents the total hazard index ($HI_{total} = HI_{inhalation} + HI_{ingestion} + HI_{dermal}$). An HI value higher than one implies that the non-cancer risk merits attention and indicates that adverse health effects are likely to occur (Dahmardeh Behrooz et al., 2021).

$$HQ_i = \frac{ADD_i}{R_fD_i} \qquad (Eq.~~6~~11)$$

$$HI_i = \sum HQ_{ij} \qquad (Eq.~~7~~12)$$

The carcinogenic risks (CR) are estimated using Eq. ~~8-10~~13-15, which refers to the probability that a person might develop a cancer over a lifetime because of exposure to a carcinogenic chemical (Dahmardeh Behrooz et al., 2021; Fadel et al., 2022a, 2022b). According to the USEPA, a cancer risk value between 10^{-6} (one additional case per one million people) and 10^{-4} (one in a ten thousand) indicates that the carcinogenic risk is considered as tolerable while a value higher than 10^{-4} indicates that a serious risk of cancer exists (Bari and Kindzierski, 2016; Dahmardeh Behrooz et al., 2021). CR_{total} represents the total carcinogenic risk ($CR_{total} = CR_{ingestion} + CR_{inhalation} + CR_{dermal}$).

$$CR_{ingestion} = ADD_{ingestion} \times CSF \qquad (Eq.~~8~~13)$$

$$CR_{inhalation} = EC_{inhalation} \times IUR \qquad (Eq.~~9~~14)$$

$$CR_{dermal} = ADD_{dermal} \times CSF \qquad (Eq.~~10~~15)$$

In the equations above CSF is the cancer slope factor for a chemical in a specific exposure pathway (mg/kg per day) and IUR is the inhalation unit risk (m^3/mg) (**Table S1**).

2.5 Source apportionment

The USEPA PMF v5.0 software was used to identify and quantify the major emission sources in Montréal. PMF is a multivariate factor analysis tool that decomposes a data matrix X (n x m) into two matrices: source contributions G (n x p) and sources profiles F (p x m), where n is the number of samples, m is the number of species and p is the number of factors or sources. The PMF model requires the concentration data set of the samples and associated uncertainty as inputs. The goal is to solve the chemical mass balance (Eq. ~~11~~16) between the measured species concentrations and source profiles:

$$x_{ij} = \sum_{k=1}^{p} g_{ik} f_{kj} + e_{ij} \qquad \text{(Eq. ~~11~~16)}$$

where x_{ij} is the concentration of the species j in the i^{th} sample~~s~~, g_{ik} is the contribution of the k^{th} source in the i^{th} sample~~s~~, f_{kj} is the relative concentration of species j from the source k, and e_{ij} is the residual of species j in the i^{th} sample. The values of g_{ik} and f_{kj} are adjusted until a minimum value of Q (Eq. ~~12~~17) for a given number of factors p is found:

$$Q = \sum_{i=1}^{n} \sum_{j=1}^{m} \left(\frac{e_{ij}}{u_{ij}}\right)^2 \qquad \text{(Eq. ~~12~~17)}$$

where e is the residual value and u is the uncertainty in a measurement. The residual value is the difference between the measured value and the PMF-modeled concentration of each compound. In the present work, samples below the detection limit (DL) were replaced by half of the DL and were given an uncertainty of 5/6 times the detection limit (Polissar et al., 1998). Missing samples were replaced by the median value of that species and were given an uncertainty of 4 times the median value (Polissar et al., 1998). When the concentration was greater than the DL, the uncertainty was calculated according to the USEPA guidelines (USEPA, 2014; Lee et al., 2022; Park et al., 2019): $\sqrt{(Concentration\ x\ 0.1)^2 + (0.5\ x\ DL)^2}$

After screening the integrity of the input data, 27 species were included in the PMF model. The overall number of samples (80 samples) and the number of species complies with the ratio of at least 3:1, as proposed by Belis et al., (2019). The species included were OC and EC, major water-soluble ions (Na^+, Cl^-, NH_4^+, NO_3^- and SO_4^{2-}) and a selection of elements (Al, Fe, Ti, Cu, Sb, Cd and Co). Levoglucosan was included as a tracer for biomass burning, 17α[H]-21β[H]-Hopane as a tracer for vehicular emissions, fatty acids (hexadecanoic acid and octadecanoic acid) for cooking activities, a set of n-alkanes for biogenic (C27, C29) and anthropogenic emissions (C20, C21, C24, C25), and finally a dicarboxylic acid (oxalic acid) and α-pinene oxidation products (pinic acid and cis-pinonic acid) as tracers for SOA.

All the included species were defined from weak to strong in the PMF model based on their signal-to-noise ratio (S/N). When the S/N ratio was less than 0.2, the PM species were classified as "bad," "weak" when the S/N ratio was between 0.2 and 2, and "strong" when the S/N ratio was greater than 2 (Esmaeilirad et al., 2020). The bad species are excluded from the analysis while the uncertainty for the weak species is tripled. $PM_{2.5}$ was designated as a "total variable" and was automatically classified as "weak". All the included species were successfully modeled by PMF with their concentrations reconstructed accurately and were qualified as "strong" except for nitrate which presented a S/N ratio of 0.9 and was defined as "weak".

The final solution was selected based on several criteria such as (1) comparison of the resulting source profiles against the literature, (2) lack of correlation between the resolved factors, (3) correlation between the predicted vs measured $PM_{2.5}$ concentrations (4) correlation between the modeled and measured species concentrations (R^2 higher than 0.8), (5) maximum individual mean (IM) and maximum individual standard deviation (IS) (**Fig. S1**). The R^2 between the reconstructed and measured $PM_{2.5}$ mass was 0.87 (slope=0.90) (**Fig. S2**). The robustness of the PMF solution was tested by the two-error estimation method (bootstrap and displacement) as instructed in the PMF manual to ensure the solution was stable (**Table S2**) (USEPA, 2014).

2.6 GEOS-Chem Simulations

~~We performed simulations~~ Simulations were performed using the GEOS-Chem chemical transport model (version 14.0.1, doi:10.5281/zenodo.7271960) (Bey et al., 2001, Park et al., 2004). GEOS-Chem is driven by assimilated meteorology from the Modern-Era Retrospective analysis for Research and Applications, Version 2 (MERRA-2), at the NASA Global Modeling and Assimilation Office (GMAO). The atmosphere was resolved using 47 vertical layers from the surface to 0.01 hPa. The vertical resolution of the model is about 100 m near the surface, but it becomes coarser at higher altitudes. Boundary conditions~~We~~ were generated ~~boundary conditions~~ using a global simulation at 2° latitude x 2.5° longitude resolution. ~~We then used a~~A nested grid is then used with 0.5° latitude x 0.625° longitude resolution, spanning 35° N to 65° N, 90° W to 50° W (**Fig. S3**) in order to include the full province of Qu~~é~~ebec as well as the strong source regions of the Great Lakes region and the northeastern US. We use the recently developed treatment of wet scavenging described by Luo et al. (2020, 2019), which has been previously shown to yield better agreement for nitrate and ammonium concentrations over eastern North America.

Biomass-burning emissions were simulated from the Copernicus Atmosphere Monitoring Service Global Fire Assimilation System (GFAS, Kaiser et al., 2012). We used global emissions from the Community Emissions Data System version 2 (CEDS v2, O'Rourke et al., 2021, Hoesly et al., 2018), except where overwritten by regional emissions inventories, as described in Keller et al. (2014). These regional emissions inventories included anthropogenic emissions from the US and most of Canada up to 54° N, provided by the National Emissions Inventory for 2016 (EPA, 2021a), with annual scaling factors to account for changes in emissions since 2016 (EPA, 2021b). Shipping emissions were provided by CEDS v2, and

aircraft emissions were provided by the Aviation Emissions Inventory Code (AEIC, Stettler et al., 2011, Simone et al., 2013). Anthropogenic emissions of fine dust aerosols were from the Anthropogenic Fugitive, Combustion, and Industrial Dust (AFCID) inventory (Philip et al., 2017), while natural dust emissions were calculated according to the Mineral Dust Entrainment and Deposition (DEAD) parameterization (Zender, 2003). Formation of SOA was parameterized using the "simple" SOA scheme that treats all organic aerosol as non-volatile, as described in Pai et al. (2020). It has been shown to reproduce observed organic aerosol concentrations with similar skill to a more complex scheme. GEOS-Chem resolves mineral dust in four size bins spanning radii of 0.1-1.0, 1.0-1.8, 1.8-3.0, and 3.0-6.0 µm. In this study, ~~we will approximate~~ the concentration of dust in particles smaller than 2.5 µm in diameter is estimated by adding 38 % of the concentration of dust in the 1.0-1.8 µm size bin to the concentration of dust in the 0.1-1.0 µm size bin (Fairlie et al., 2010, Zhang et al., 2013). GEOS-Chem has previously been evaluated against NO_2 concentrations from the USEPA Air Quality System sites (Silvern et al., 2019), satellite observations of aerosol optical depth, speciated aerosol concentrations from aircraft measurements over the United States (US) and speciated surface observations from the USEPA Chemical Speciation Network (CSN), Interagency Monitoring of Protected Visual Environments (IMPROVE), and the Southeastern Aerosol Research and Characterization (SEARCH) Network (Kim et al., 2015), and ozone concentrations from the Clean Air Status and Trends Network (CASTNet, Reidmiller et al. 2009). In all cases, GEOS-Chem has been shown to adequately resolve emissions, atmospheric processes, and large-scale transport. The model performance was evaluated against the observations presented in this study and good correlation with the observed values was obtained (R=0.24-0.76) (**Table S3**). Some of the indicators are not within the acceptable limits (Abdallah et al., 2018) and this is likely because of the vertical and horizontal resolution of the model. Thus, the PMF results and the model outputs will be compared qualitatively. Furthermore, GEOS-Chem results have been previously used for source contribution analysis similar to the analysis presented in this study (Meng et al. 2019).

In order to examine the sensitivity of air pollutant concentrations to contributions from source regions, ~~we perform~~ a base-case simulation is performed along with ~~and~~ three sensitivity simulations, each with anthropogenic emissions from a geographic region turned off: noQC, noCA, and noUS. In the noQC simulation, ~~we do not allow any~~ anthropogenic emissions within the borders of the province of Québec are not allowed. In the noCA simulation, ~~we do not allow any~~ anthropogenic emissions within the borders of Canada are not allowed, except for emissions from the province of Québec (Rest of Canada, RoC). In the noUS simulation, ~~we do not allow any~~ anthropogenic emissions within the borders of the contiguous US are not allowed. Emissions from shipping and aircraft are removed within the boundaries of the specified region, but emissions ~~we have not changed emissions~~ from biomass burning or natural sources are not changed. We note that for the purposes of masking emissions, each model grid cell is considered to be entirely within one province or country; the resolution of the provincial or national masks is the same as the model resolution. By calculating the differences in the concentrations of PM components in the sensitivity simulations compared to the base-case simulation, we qualitatively evaluate the proportions of air pollutants in Québec due to sources within Québec, sources in the RoC, and sources in the contiguous US.

3 Results and discussion

3.1 $PM_{2.5}$ concentrations

The average $PM_{2.5}$ concentration (and standard deviation) at the MTL site was 4±3 µg/m^3. The concentration of $PM_{2.5}$ in all samples collected at MTL site was lower than the daily standard set by the World Health Organization (WHO) (15 µg/m^3) (WHO, 2021) and the Canadian daily standard of 27 µg/m^3 (EAR, 2019) (**Fig. 1**). The $PM_{2.5}$ levels at the MTL site can be compared against nearby government monitoring stations to understand if there are large differences in concentrations and how concentrations have changed over recent years in this area of Montréal. The average concentrations at MTL were lower than that reported during the same sampling period at Décarie station (6.6 µg/m^3) located ~5 km South-West of the MTL site near an intersection of two major highways (**Fig. 2**). Given that the Décarie station is strongly impacted by vehicle emissions, this difference is not surprising. In contrast, the average $PM_{2.5}$ concentration at the MTL site is similar to that recorded at the Molson station (NAPS ID: S50134; ~4 km North-East of MTL) (4.7 µg/m^3), which is located in a mixed residential/industrial zone for the same sampling period. Furthermore, there is a general decreasing trend between 2017 and 2020 in $PM_{2.5}$ levels at the government monitoring stations. Since the concentration of $PM_{2.5}$ in 2020 was not too different in comparison with the previous years (2018 and 2019), the sources of $PM_{2.5}$ identified in this study are likely to be similar to other years. It is important to mention that during our sampling period, Montréal was in partial lockdown where public spaces (e.g., bars, gyms, cinemas, museums, libraries and casinos) were closed due to the possibility of a second wave of the COVID-19 pandemic. Primary and some secondary schools were opened during that period. While these considerations suggest that the results presented here are also applicable to pre-and post-pandemic conditions, further studies are needed before generalizing the results of this study to other periods.

365

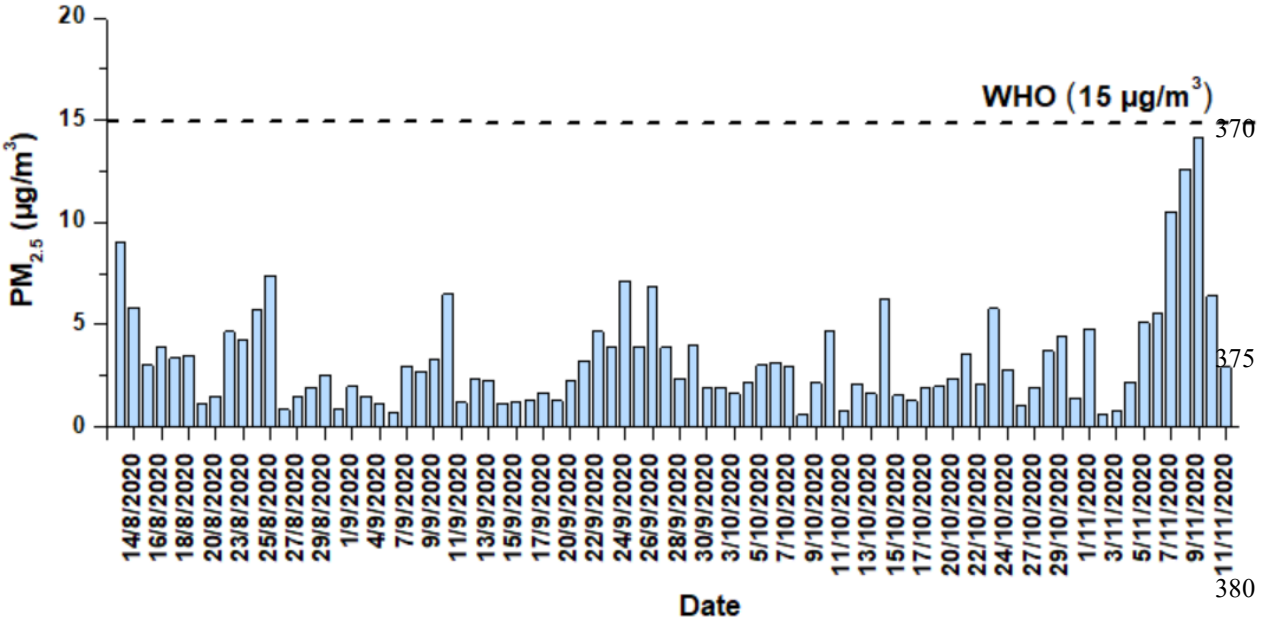

Figure 1. The temporal variation of $PM_{2.5}$ concentrations for the sampling period (13 August to 11 November 2020).

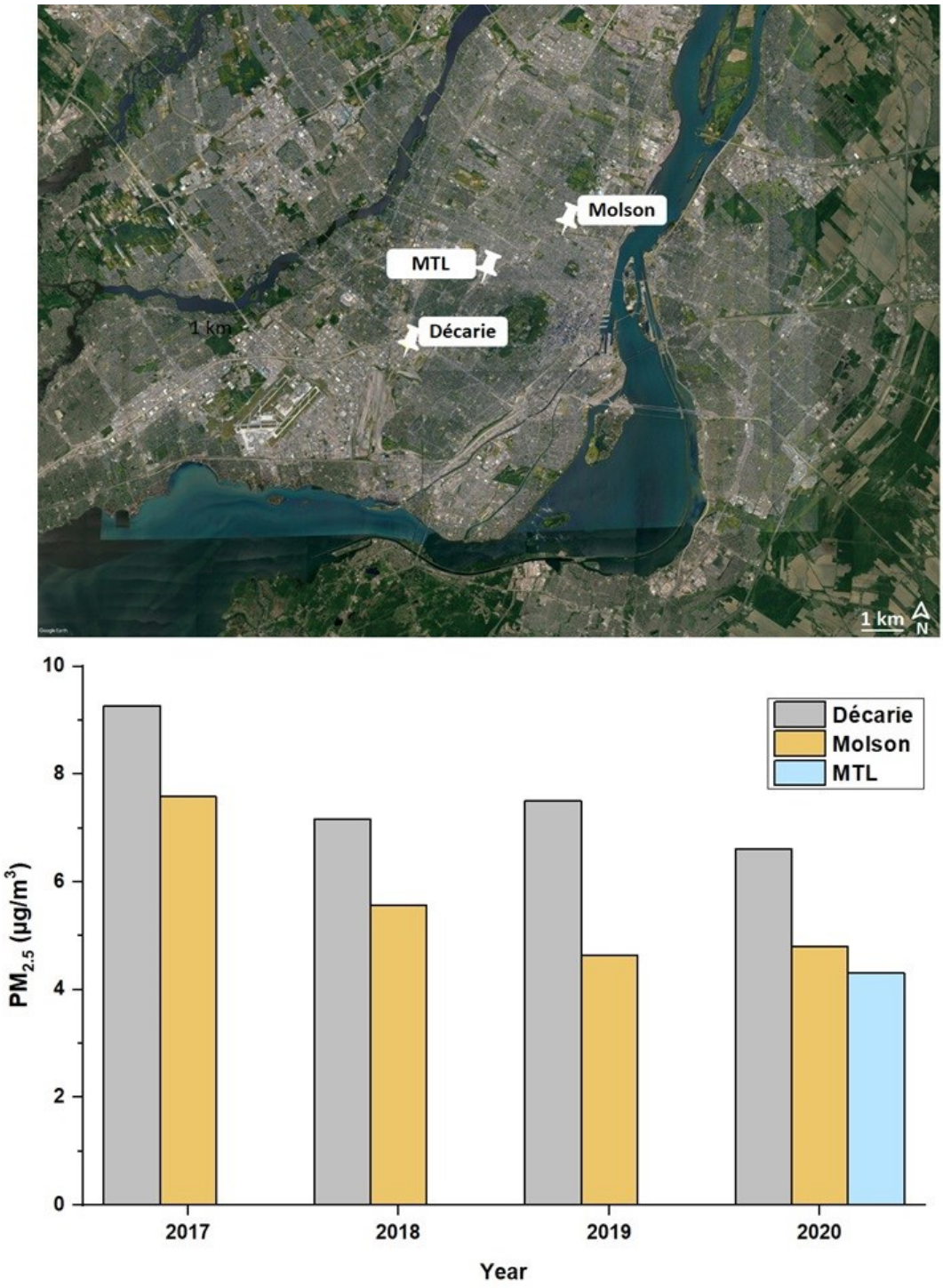

385 **Figure 2.** $PM_{2.5}$ concentrations for the sampling period (13 August to 11 November 2020) at MTL, and for Décarie and Molson sites between 2017 and 2020 along with the location of the sampling sites (Google Earth®). For Décarie and Molson sites, the data correspond to the same dates of the year (13 August to 11 November).

3.2 Carbonaceous matter

The average OC and EC concentrations (± standard deviation) were 1.31±0.76 μg/m^3 and 0.17±0.15 μg/m^3, respectively (**Table 2**). While EC originates from combustion sources and has a primary origin, OC can be directly emitted from combustion of fossil fuels, biomass burning, cooking activities, and can also be formed in the atmosphere through chemical reactions (Hallquist et al., 2009). The OC/EC ratio is a useful diagnostic ratio that provides information on the sources in $PM_{2.5}$. An OC/EC ratio ranging between 0.3 and 1 was reported for diesel vehicles, between 1.4 and 5 for gasoline operated vehicles while a larger OC/EC ranging between 4.1 and 14.5 for biomass burning (Khan et al., 2021; Salameh et al., 2015). In this study, the ratio of OC/EC was 7.4~~2~~±3.1~~2~~, which is larger than those associated with vehicular emissions and consistent with the presence of biomass burning. Indeed, wood burning may be an important source of air pollutants in Qu~~é~~ébec and wood-burning stoves and fireplaces are used in both residential and businesses settings (e.g., pizzerias and bagel factories). The production of secondary organic carbon will also increase OC/EC ratios beyond values measured for primary sources. Indirect methods have been developed for identifying primary (POC) or secondary organic carbon (SOC) (Shivani et al., 2019; Calvo et al., 2008; Joseph et al., 2012).

$$SOC = OC_{total} - EC \times \left(\frac{OC}{EC}\right)_{min} \quad \text{(Eq. ~~13~~18)}$$

One such method is summarized in Eq. ~~13~~18, OC_{total} is the measured OC and $(OC/EC)_{min}$ is the minimum ratio observed in the samples. Additional information on the calculation method is included in the supplementary material. Using this method, the average contribution of SOC to the total OC and the standard deviation was 61±15% at the MTL site indicating a strong SOC contribution.

3.3 Organic species

Some organic compounds are specific to a certain source and have been used in source apportionment studies as molecular markers. The average concentrations of selected organic compounds in $PM_{2.5}$ measured at the MTL site are summarized in **Table 3**. Levoglucosan, generated by the pyrolysis of cellulose and often utilized as a particular marker of biomass burning (Simoneit, 2002), was the most abundant compound among the organic tracers examined. Due to its presence in lubrication oil used in both gasoline and diesel vehicles, 17α(H)-21β(H)-Hopane is a specific marker of traffic emissions, and it was the least prevalent measured organic species in the $PM_{2.5}$ (El Haddad et al., 2009; Fadel et al., 2021). Arabitol and mannitol were well correlated (R=0.98; $p<0.001$) and are commonly described as markers for primary biogenic emissions, more specifically with fungal spores (Petit et al., 2019). Alkanes, specifically acyclic saturated hydrocarbons, can originate from both biogenic and anthropogenic sources. The n-alkane with the highest concentration was C29. In the literature, low molecular weight n-alkanes (<C27) are primarily associated with traffic emissions, whereas high molecular weight n-alkanes (C27, C29, C31) are associated with plant detritus because they are abundant in the epicuticular wax of plants (Rogge et al., 1993a, 1993b).

To further evaluate the contribution of the anthropogenic and the biogenic sources to n-alkanes, the carbon preference index (CPI) was calculated (Fadel et al., 2021; Esmaeilirad et al., 2020). Two CPI parameters were adopted: the Overall CPI for the whole range of n-alkanes (C15-C30), and the High CPI for the higher molecular weight n-alkanes (C25-C30). The detailed description of the calculation method is included in the supplementary material. The average Overall CPI value was 0.86±0.21, indicating the contribution of petrogenic sources. The High CPI values during the entire campaign were between 0.74 and 2.81, with a majority of the measurements in the anthropogenic range and the rest in the mixed anthropogenic/biogenic range (**Fig. 3**). The average High CPI was 1.56±0.48, indicating that larger n-alkanes at the MTL site are predominately anthropogenic with a lesser biogenic contribution.

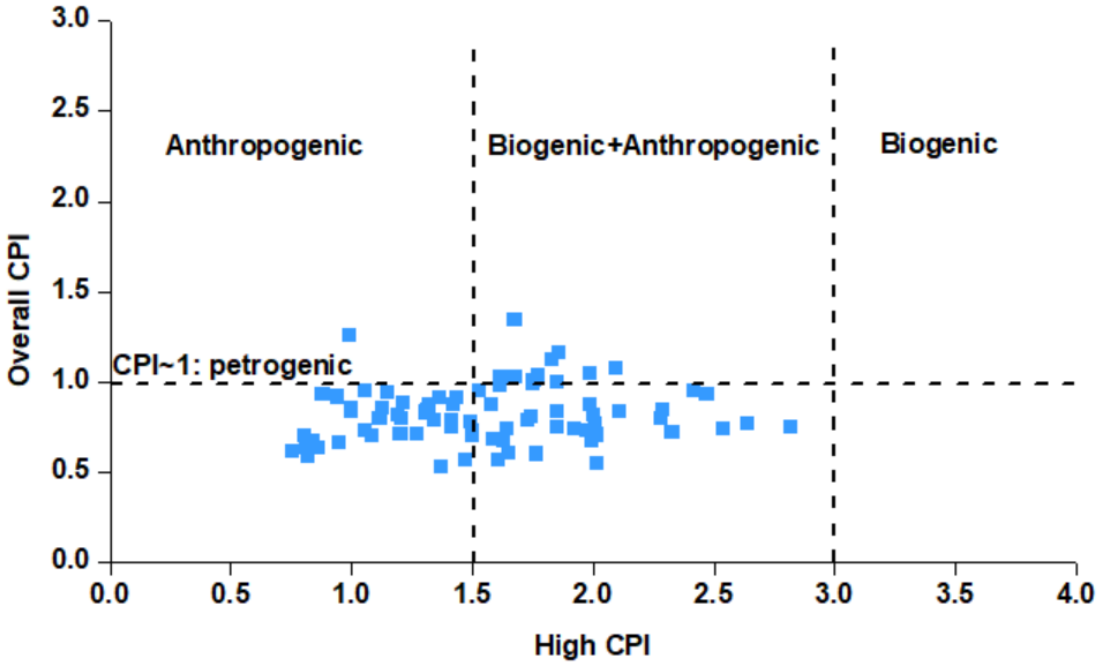

Figure 3. The n-alkanes source identification using the carbon preference index (CPI).

Table 2: Concentrations of major and trace components of $PM_{2.5}$ measured at MTL site.

	Mean	Stdev	Range
			µg/m^3
OC	1.31	0.76	0.64-4.23
EC	0.17	0.15	0.05-0.85
SO_4^{2-}	0.56	0.40	0.09-2.34
NO_3^-	0.18	0.29	0.01-2.21
NH_4^+	0.36	0.23	0.03-1.32
Na^+	0.04	0.02	0.003-0.13
Cl^-	0.03	0.03	0.003-0.13
Mg^{2+}	0.01	0.007	0.001-0.06
K^+	0.03	0.03	0.002-0.19
Ca^{2+}	0.11	0.21	0.019-1.90
			ng/m^3
Na	109.44	54.52	33.62-335.33
Mg	42.62	44.04	10.79-380.38
Ti	2.57	4.34	0.13-36.11
Al	111.17	62.45	4.93-405.3
K	69.68	36.63	21.72-283.02
Mn	2.97	2.76	0.79-24.72
Fe	76.07	101.66	0.69-932.46
Zn	39.53	38.52	14.04-240.40
Ni	1.21	0.93	0.33-6.35
Sr	1.05	1.41	0.25-11.95
Cu	15.26	19.45	0.44-101.8
Co	3.81	5.76	0.026-27.8
Cr	3.05	0.12	0.05-0.72
V	0.31	0.35	0.03-2.68
Cd	0.13	0.17	0.0004-1.21
Mo	0.30	0.13	0.13-0.99
Sb	0.25	0.21	0.04-1.20
Pb	5.66	5.41	0.63-33.4

Table 3: Average concentrations (ng/m^3) of organic compounds in $PM_{2.5}$.

	Mean	Stdev	Range
17α(H)-21β(H)-Hopane	0.18	0.01	0.06-0.70
n-Alkanes			
Tetradecane (C14)	0.58	0.31	0.20-1.73
Pentadecane (C15)	0.48	0.66	0.28-4.27
Hexadecane (C16)	0.75	0.37	0.34-2.04
Heptadecane (C17)	0.71	0.67	0.22-5.20
Octadecane (C18)	0.99	1.69	0.18-8.29
Nonadecane (C19)	0.46	0.24	0.17-1.26
Eicosane (C20)	1.82	1.20	0.73-7.90
Heneicosane (C21)	0.99	0.35	0.37-2.14
Docosane (C22)	0.96	1.15	0.37-8.49
Tricosane (C23)	1.02	0.42	0.40-2.16
Tetracosane (C24)	2.24	1.61	0.82-11.16
Pentacosane (C25)	1.97	1.02	0.83-4.97
Hexacosane (C26)	1.51	0.84	0.48-3.96
Heptacosane (C27)	2.52	2.89	0.74-23.82
Octacosane (C28)	1.79	2.84	0.45-23.20
Nonacosane (C29)	3.84	3.78	0.73-3.37
Triacontane (C30)	1.12	1.41	0.12-7.07
Hentriacontane (C31)	1.56	0.96	0.34-6.72
Sugars			
Levoglucosan	33.72	6.45	6.45-126.40
Mannosan	1.03	0.94	0.15-4.59
Mannitol	2.14	3.22	0.23-18.91
Arabitol	3.14	4.29	0.29-39.00
Glucose	2.92	3.01	0.17-24.47
Fatty acids			
Tetradecanoic acid	4.17	1.40	1.66-7.97
Hexadecanoic acid	51.12	13.09	28.39-87-43
Octadecanoic acid	37.06	9.41	18.05-64.90
Oleic acid	4.43	1.65	2.51-13.05
Dicarboxylic acids (DCAs)			
Oxalic acid (diC2)	7.79	1.58	0.28-15.03
Adipic acid(diC6)	1.60	4.18	0.31-3.42
Azelaic acid (diC9)	5.93	2.18	1.12-15.01
Biogenic SOA Tracers			
Pinic acid	4.73	1.78	0.21-8.93
Cis-pinonic acid	3.17	1.71	0.62-9.73

3.4 Elemental composition

~~To differentiate between the anthropogenic and natural origins of the various elements, the EF was determined. As shown in **Fig. 4**, Ti, Fe, Mg, V, K, Sr, Mn, Na and Ni presented EF values lower than 10, indicating that these elements mainly originate from crustal sources. In contrast, Cr, Co, Mo, Cu, Pb, Cd, Zn and Sb exhibited high enrichment factors, indicating that these elements are predominately from anthropogenic sources. Moreover, a significant correlation (R>0.95, $p<0.05$) was observed among Ti, Fe, Mg, V, K, Mn and Na, indicating a common crustal source.~~

The relationship between trace metals provides qualitative information on the sources of the measured elements. A significant correlation (R>0.95, $p<0.05$) was observed among Ti, Fe, Mg, V, K, Mn and Na, indicating a common crustal source. Numerous studies have analyzed the chemical composition of traffic-related PM and have reported that Cu, Sb and Cd are linked to non-exhaust emissions, more precisely from vehicular brake wear (Thorpe and Harrison, 2008; Lin et al., 2015; Pio et al., 2013; Mancilla et al., 2012; Pant et al., 2013). In this study, a correlation of R=0.82 ($p<0.05$) was found between Sb and Cd indicating that Sb and Cd originate from the same sources, most probably brake wear. Studies in other Canadian cities, namely Toronto and Vancouver, have also associated the elements Sb and Cd with non-exhaust emissions from road traffic (Celo et al., 2021). No correlation was found between Cu and the elements Cd and Sb (R<0.01, $p<0.05$); indicating that brake wear debris was not an important source of Cu in Montréal.

Additionally, Co was correlated with Cr (R=0.79, $p<0.01$) and Cu (R=0.86, $p<0.05$), suggesting a common source from industrial emissions, similar to observations in Edmonton, Canada (Bari and Kindzierski, 2016). The Canadian Copper Refinery and Suncor Energy refinery can be identified as potential sources of Cr and Co in the Montréal region based on the National Pollutant Release Inventory (NPRI) data published by the Government of Canada (NPRID, 2022). It is important to mention that Cu, Cr and Co could also originate from other sources such as traffic-related emissions and coal combustion (Riffault et al., 2015; Bari & Kindzierski, 2016; Thorpe & Harrison, 2008; Celo et al., 2021). However, these possibilities seem less important given the correlations between the elements as well as the lack of coal combustion in the province of Québec. Lastly, no correlation was found between Zn, Pb and Sb with Cl^- (R<0.09, $p<0.05$) revealing that incinerators are not a potential source of these trace elements (Riffault et al., 2015; Rahn and Huang, 1999).

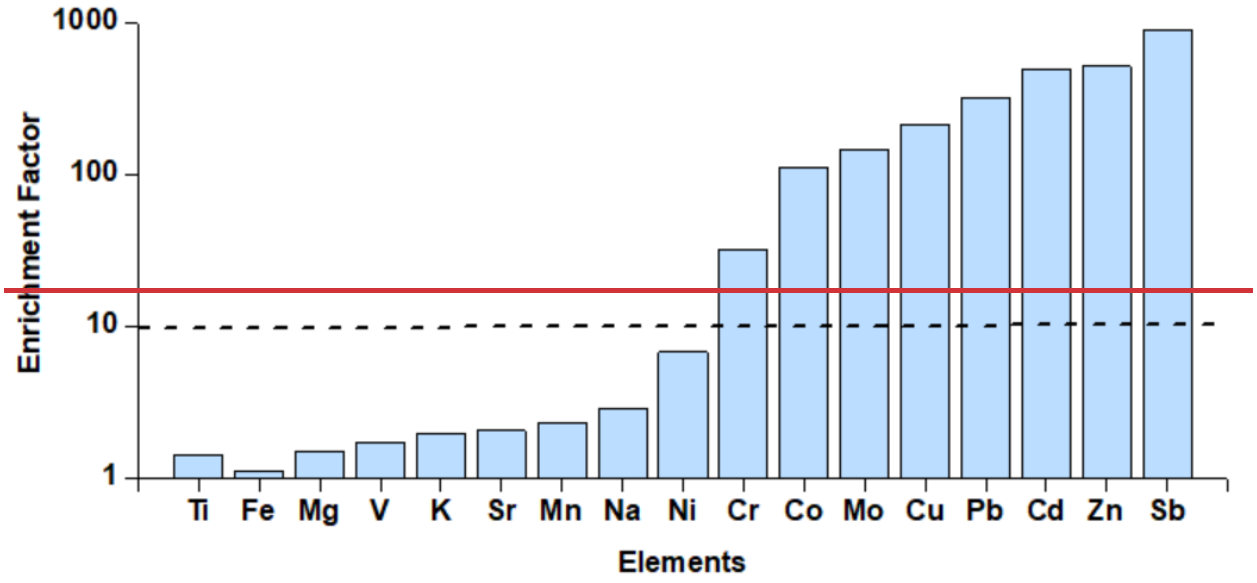

Figure 4. Enrichment factor of selected elements in $PM_{2.5}$. An EF higher than 10 indicates an anthropogenic source.

475

3.5 Water-soluble ions

Among the water-soluble ions, SO_4^{2-} presented the highest concentration followed by NH_4^+, NO_3^-, Ca^{2+}, Na^+, Cl^-, K^+, and the species with the lowest concentration was Mg^{2+}. The secondary inorganic aerosol components (sulfate, ammonium, and
480 nitrate) accounted for 83% of the total water-soluble ions and 32% of the total $PM_{2.5}$ mass (**Fig. S5**). The presence of secondary sulfate is supported by the strong correlation between sulfate and ammonium with a Pearson coefficient of 0.90 ($p<0.005$). This result, and the weak correlation between ammonium and nitrate (R=0.27, $p<0.002$), suggests that a significant fraction of ammonium in $PM_{2.5}$ was associated with ammonium sulfate with a limited amount of ammonium nitrate. Nitrate concentrations were higher in the end of October and November in comparison with the warmer months (**Fig.**
485 **S6**) consistent with a shift in equilibrium partitioning from gas-phase nitric acid to the particle-phase nitrate due to colder temperatures (Geng et al., 2013; Mantas et al., 2014). The Total Ammonium/Total Sulphate (TA/TS) molar ratio was used to evaluate if the site conditions were ammonia-rich (>2) or ammonia-poor (<2) (Joseph et al., 2012; Remoundaki et al., 2013). The TA/TS molar ratio was 1.24, highlighting that the concentrations of ammonium are not sufficient to neutralize the concentrations of sulfate and nitrate. Therefore, the latter anions could be associated to different cations such as Na^+, Mg^{2+},
490 K^+ and Ca^{2+} and the formation of salts with these cations (e.g., $NaNO_3$, $MgSO_4$). Moreover, when considering the neutralization of all the cations (Na^+, Mg^{2+}, NH_4^+, K^+, Ca^{2+}) by all the anions (SO_4^{2-}, NO_3^-, Cl^-), the scatter plot (**Fig. S7**) presented a slope of 0.98, indicating a charge balance between the anions and cations.

3.6 Source apportionment of $PM_{2.5}$

3.6.1 Source identification

The source profiles obtained from the PMF model are presented in **Fig. ~~5~~4**. Eleven sources were identified at MTL site namely SOA, secondary inorganic aerosol, crustal dust, marine, biomass burning, cooking, traffic exhaust, road dust, industrial, plant wax and biogenic SOA. The species with the highest loadings were used to identify each factor, and comparison to source profiles found in the literature served as confirmation.

The SOA factor was distinguished with high loading of oxalic acid (75% of the total concentration of oxalic acid) and contributed to 22% of the $PM_{2.5}$ mass concentration (Petit et al., 2019). Oxalic acid is a byproduct of oxidation from various precursors including biogenic (e.g., isoprene) and anthropogenic (e.g., cycloalkanes) compounds, and it is also generated from the photochemical oxidation of larger acid homologues (Srivastava et al., 2019).

The secondary inorganic aerosol (SIA) factor was distinguished by the presence of the water-soluble ions SO_4^{2-} (58%) and NH_4^+ (59%). This factor accounted for 17% of the total $PM_{2.5}$. No trend was observed in the time series of this factor and this source can originate from both local emissions and long-range transport (LRT) originating from the rest of Canada (e.g., Ontario) and the United States (Seinfeld and Pandis, 2016; NPRID, 2022). Aluminum production and industrial processes related to metallurgy and all other minor sources contributed to ~ 90 000 tons of SO_2 in Québec in 2020, which consists of 15% of the total Canadian emissions (583 008 tons) (NPRID, 2022). Although based on the weak correlation between sulfate and Al and strong correlation of Al with crustal elements, we believe that aluminium production is not an important source of particulate aluminum at our site.

The crustal dust factor was identified by high loadings of Al (68%), Fe (76%) and Ti (63%). This factor accounted for 12% of the total $PM_{2.5}$ and is likely associated with crustal dust sources such as wind-driven resuspension, construction and agricultural activities (Bari and Kindzierski, 2016). All of these crustal dust sources are plausible given that construction is omnipresent in Montréal, and the surrounding St. Lawrence Valley has a large amount of agriculture.

A marine factor was characterized by the ions Na^+ (46%), Cl^- (69%) and NO_3^- (30%), contributing to 11% of the $PM_{2.5}$. The Cl^-/Na^+ calculated for this factor was 0.95, which is lower than the ratio of 1.80 reported for fresh sea-salt and is indicative of aged sea-salt (Petit et al., 2019; Seinfeld and Pandis, 2016). The presence of high nitrate loading in the profile further confirms the presence of aged marine salt. The observed chloride depletion is due to the reaction of nitric and sulfuric acid with NaCl particles (Seinfeld and Pandis, 2016).

Biomass burning was identified by high loadings of levoglucosan (70%) (Fadel et al., 2023). The OC/EC in this factor was 8.4, consistent with biomass burning (Khan et al., 2021). This source accounted for 9% of the total $PM_{2.5}$ mass. Levoglucosan is a major pyrolysis product of cellulose and hemicellulose (Simoneit, 2002), and has been used as a molecular marker of biomass burning aerosols in several source apportionment studies (Gadi et al., 2019; Shivani et al., 2019). No trend was observed in the time series of this factor with season or temperature, indicating that levoglucosan originates from both residential burning and forest fires.

A cooking emissions factor was identified based on the contribution of hexadecanoic (65%) and octadecanoic acids (68%) in the profile and accounted for 9% of the total $PM_{2.5}$ mass. These carboxylic acids have been used in source apportionment studies to distinguish cooking activities (Gadi et al., 2019; Lv et al., 2021; Shivani et al., 2019).

The traffic exhaust factor was identified by the presence of 17α[H]-21β[H]-Hopane and lower molecular weight n-alkanes (C20 to C25) and accounted for 6% of total $PM_{2.5}$ mass concentration. Hopanes are specific markers of traffic emissions due to their presence in lubrication oil (Rogge et al., 1993a; Schauer et al., 2002). Furthermore, dynamometer tests results showed that the most abundant n-alkanes were C20 and C21 for diesel vehicle emissions and C24 – C25 for gasoline-powered vehicle emissions (Rogge et al., 1993a), and these compounds are commonly associated with motor vehicle emissions. This traffic exhaust factor contributed around 72% of the hopane mass in the model, 59% of the C24 mass and 62% of the C25 mass. We suggest that the traffic emission factor is comprised principally of primary exhaust emissions given the lack of secondary tracers in the factor profile.

The road dust factor was characterized by high loadings of Cd (69%) and Sb (58%) and accounted for 2% of $PM_{2.5}$. These elements are linked to non-exhaust vehicle emissions, particularly from brake-wear debris (Thorpe and Harrison, 2008; Lin et al., 2015).

The industrial emissions factor was dominated by Cu and Co and contributed 70% and 90% of the mass of these elements, respectively, and accounted for 6% of $PM_{2.5}$. These elements are emitted from metal-industry related sources and coal combustion (Riffault et al., 2015; Bari and Kindzierski, 2016; Sharma and Mandal, 2017), but coal is not used for electricity generation in Québec and thus industrial sources seem more likely to be responsible for this factor.

The plant wax factor was characterized by high loadings of C27 and C29 with 55% of the C27 and 58% of the C29 apportioned to this factor (Fadel et al., 2023). These compounds have been previously linked to primary biogenic emissions (Rogge et al., 1993b). This factor contributed to 2% of the total $PM_{2.5}$.

Finally, the biogenic SOA factor accounted for 75% of the measured pinic acid and 66% of the measured pinonic acid and accounted for 4% of $PM_{2.5}$. α-Pinene is one of the most atmospherically important compounds in the monoterpene family, and pinic acid and pinonic acid are derived from the photooxidation of α-pinene with ozone (O_3) and hydroxyl (OH) radicals (Fadel et al., 2021). Although it is uncommon to see these species included in PMF models, doing so provides insight into how much biogenic SOA contributes to $PM_{2.5}$ mass concentration.

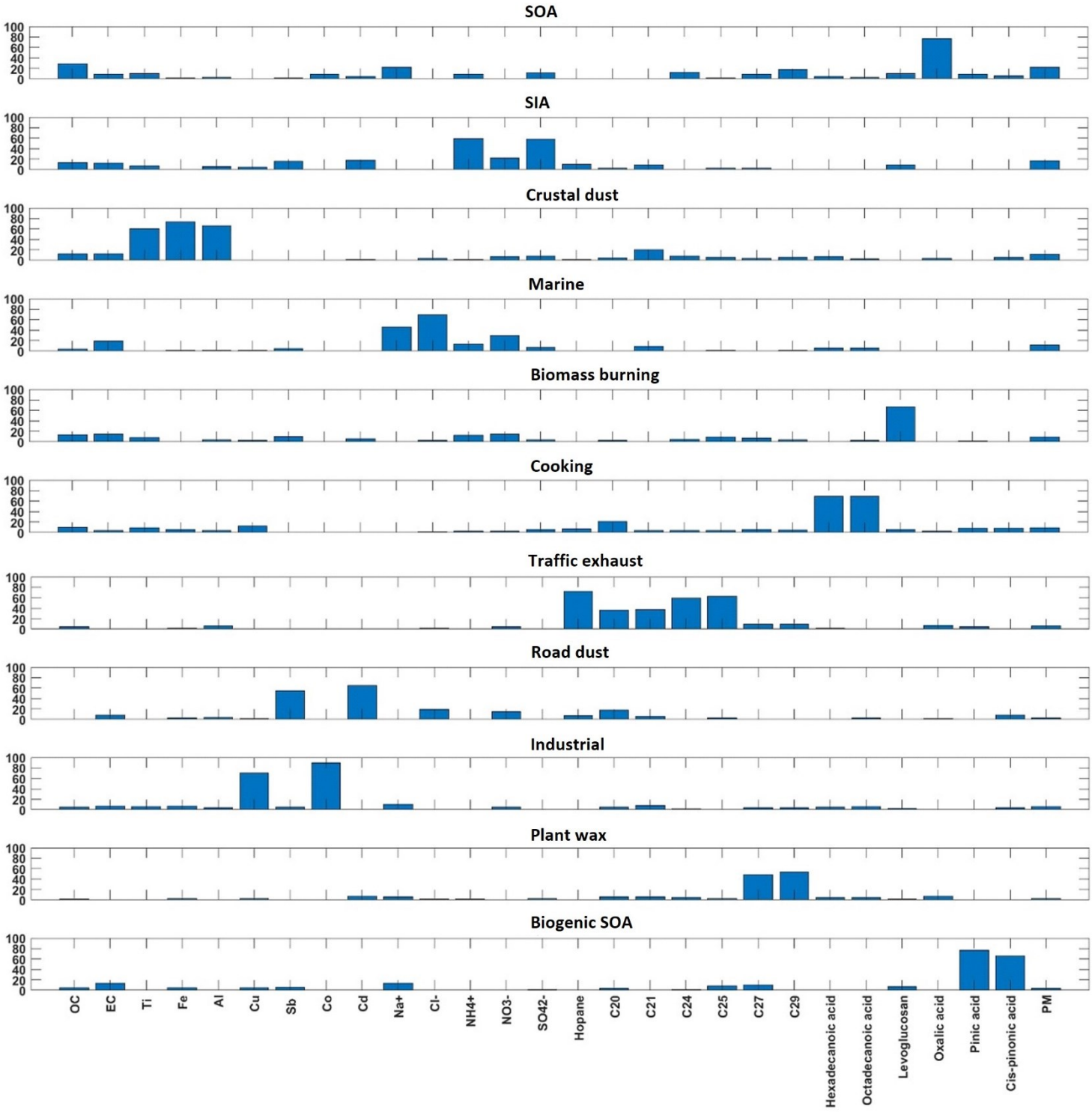

Figure 5. Profiles of the eleven factors identified from the PMF model. Loading (in percentage) is indicated on the vertical axes.

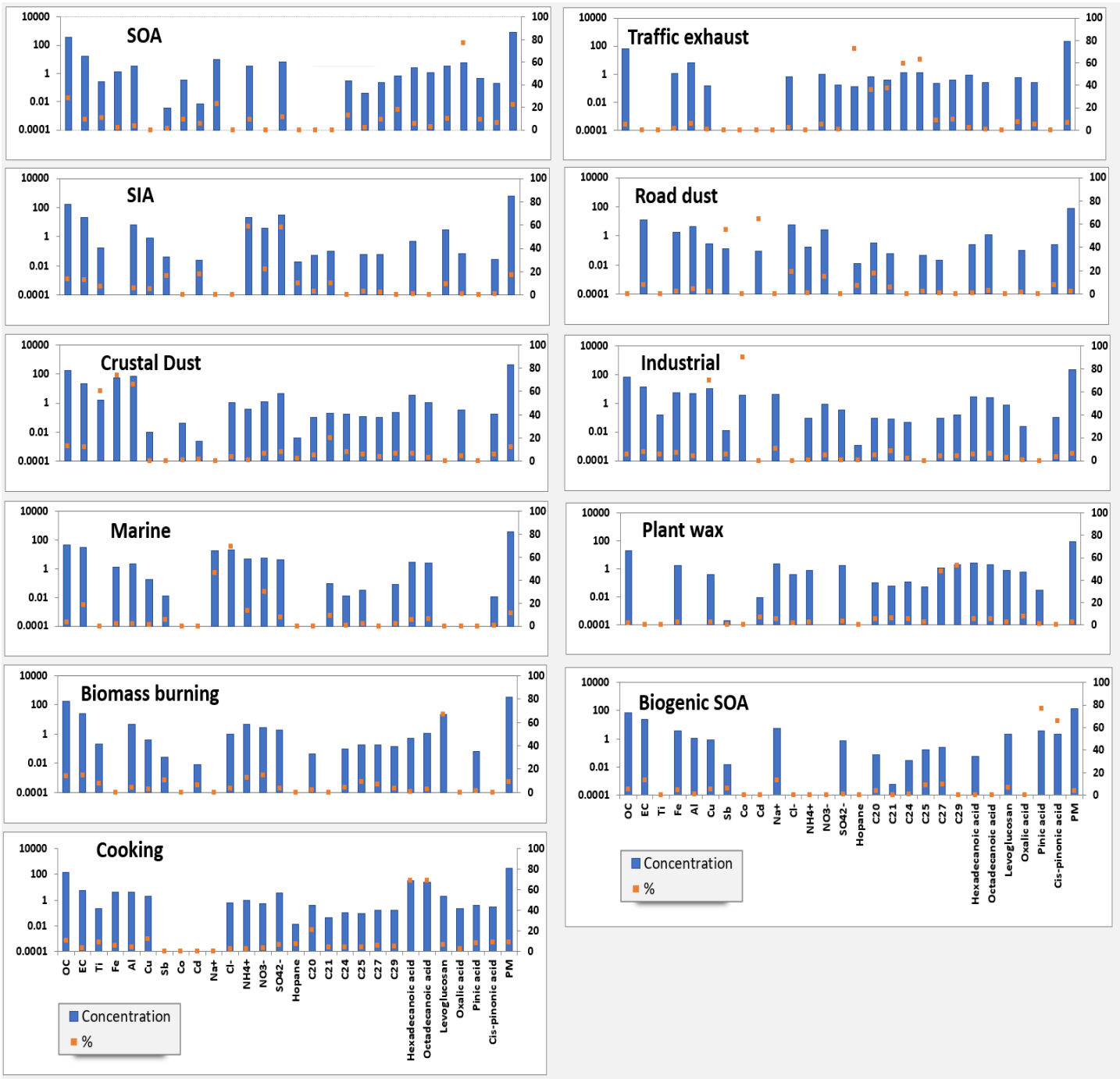

555

Figure 4. Profiles of the eleven factors identified from the PMF model. The left axis corresponds to concentration (blue bars) and the right axis percentage (orange markers). Units of concentration are ng/m^3.

3.6.2 Source contribution to $PM_{2.5}$

One of the originalities of the present study relies on the identification of primary and secondary biogenic and anthropogenic sources based on the inclusion of selected organic markers in the PMF model namely n-alkanes, anhydrosugars, a hopane, fatty acids, dicarboxylic acids, and biogenic secondary organic aerosols tracers. Of a total of 11 sources, the addition of organic markers allowed the identification of 4 of them, namely SOA, cooking, plant wax, and biogenic SOA.

When the $PM_{2.5}$ sources identified in this study were compared to other source apportionment studies conducted in major urban areas in Canada (Bari & Kindzierski, 2016; Jeong et al., 2011; Celo et al., 2021) where NAPS $PM_{2.5}$ chemical speciation datasets were used as inputs, this work resolved additional primary and secondary biogenic and anthropogenic sources due to the inclusion of a large suite of organic markers in the PMF model that were not available previously. The additional sources identified, namely SOA, BSOA, plant wax, cooking emissions are also rarely apportioned in the literature (Gadi et al., 2019; Lv et al., 2021).

There are also important differences between the source profiles for vehicular emissions in this study versus previous source apportionment studies conducted in Canada. In Montréal for example, Jeong et al. (2011) identified a traffic emission factor based on the contributions of OC, EC and oxalate. On the other hand, the traffic factor was identified in Edmonton based on the contribution of Ba, Sb, EC, Cu and Co (Bari and Kindzierski, 2016). Since trace elements and carbonaceous matter could be emitted from a variety of sources, this study refined the evaluation of vehicular sources by incorporating two source-specific organic tracers in the PMF model, namely n-alkanes and a hopane. This allowed the differentiation of exhaust and non-exhaust emissions.

The PMF results indicate that SOA and SIA were the largest contributors to fine PM and together constituted 39% (1.68 $\mu g/m^3$) of the measured $PM_{2.5}$ mass (**Fig. ~~6~~5**). The primary local urban anthropogenic sources, namely traffic exhaust, road dust, industrial and cooking emissions contributed to 23% (0.99 $\mu g/m^3$) of the measured $PM_{2.5}$ mass. These sources along with crustal dust, biomass burning, and plant wax comprise the primary aerosol fraction that is 44% (1.94 $\mu g/m^3$) of the measured $PM_{2.5}$ mass. It should also be noted that residential burning likely contributes to the biomass burning factor, but this factor is not included with the primary local urban anthropogenic sources listed above since it is not possible to distinguish residential burning from wildfires in our PMF analysis. Pollution rose plots (Figure S10) were used to analyze the correlations between wind direction and factor concentrations by plotting in a polar graph the frequency of different concentrations of a factor as a function of wind direction. Such analyses provided information on the potential local origin of the factors. Additional information is included in the supplementary material.

The chemical transport model GEOS-Chem was used to qualitatively evaluate the relative contributions from three different source regions, namely Québec, RoC, and United States to the sources (**Fig. S4**). To link the modelling results to the PMF factors, we focus on modelled concentrations of SOA, of dust in particles smaller than 2.5 µm in diameter, and of the sum of NH_4 and SO_4. As most of the NH_4^+ and SO_4^{2-} was observed to be in the SIA PMF factor, we expect the sum of the simulated

concentrations of NH_4 and SO_4 from GEOS-Chem have similar sources as the SIA PMF factor. Similarly, the concentrations of SOA from GEOS-Chem would be analogous to the sum of the SOA and biogenic SOA factors, although we note that only anthropogenic sources were altered in the sensitivity simulations. The dust species in GEOS-Chem comprises not only road dust and crustal dust, but all elements not included in the other model aerosol species (primary and secondary organic aerosol, elemental carbon, sulfate, nitrate, ammonium, and sea-spray aerosol). It is therefore most comparable to the sum of the crustal dust, road dust, and industrial PMF factors. Together, the SIA, SOA, biogenic SOA, crustal dust, road dust, and industrial PMF factors comprise 61% of the total observed $PM_{2.5}$ mass.

According to the findings of the chemical transport modelling, Montréal air pollution concentrations are influenced by all three of the regions that were considered. As presented in **Fig. ~~7~~6**, the US makes an important contribution to SOA and ammonium sulfate concentrations. The concentrations of SOA dropped by 22% between the base case and the sensitivity simulation without Qu~~é~~ébec emissions and by 36% when the US emissions were not included. The concentrations of ammonium sulfate decreased by 33% when US emissions were excluded and by 35% when emissions from Qu~~é~~ébec were excluded. Thus, GEOS-Chem simulations reveal an important contribution from US emissions to ammonium sulfate and SOA concentrations.

On the other hand, anthropogenic dust emissions from Québec presented the highest contribution to total dust concentrations and the concentrations dropped by 16% when emissions from Qu~~é~~ébec were excluded and by 10% when US emissions were excluded. The sum of the anthropogenic fractions is 30% for dust in GEOS-Chem, which is close to the ratio of the $PM_{2.5}$ mass in the industrial and road dust PMF factors to the sum of the industrial, road dust, and soil dust factors (40%). The similarity in the two approaches (modeling versus PMF) increases confidence that the dust sources are being correctly apportioned in our study. In general, emissions from the RoC for all pollutants presented a smaller contribution to local concentrations than Qu~~é~~ébec or US emissions (**Fig. ~~7~~6**). Therefore, GEOS-Chem emphasized the important role of transboundary input from the US during our sampling period. $PM_{2.5}$ can be reduced through local mitigation strategies, but the effectiveness of such strategies will be limited without updating international agreements to further reduce transboundary pollution.

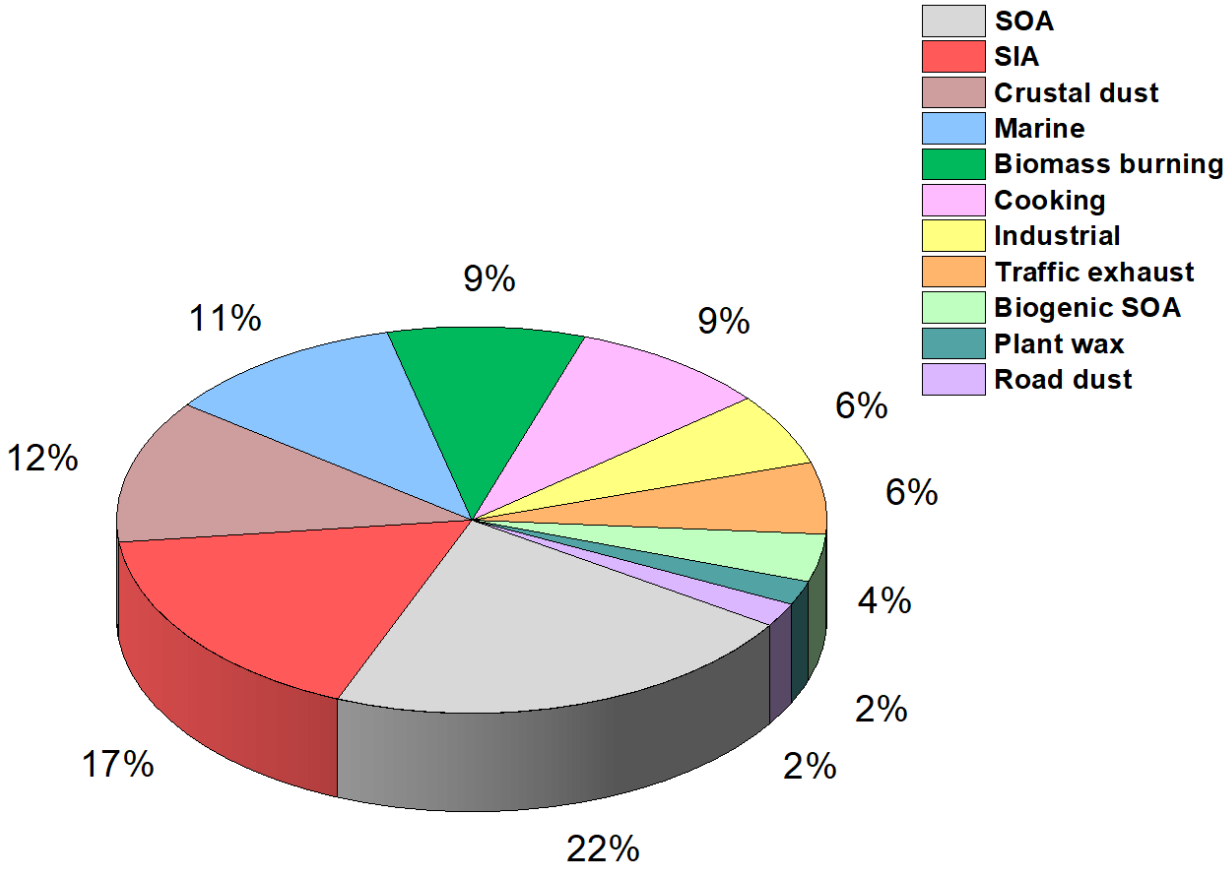

Figure ~~6~~5. Contributions of the eleven identified sources to the total $PM_{2.5}$ mass.

620

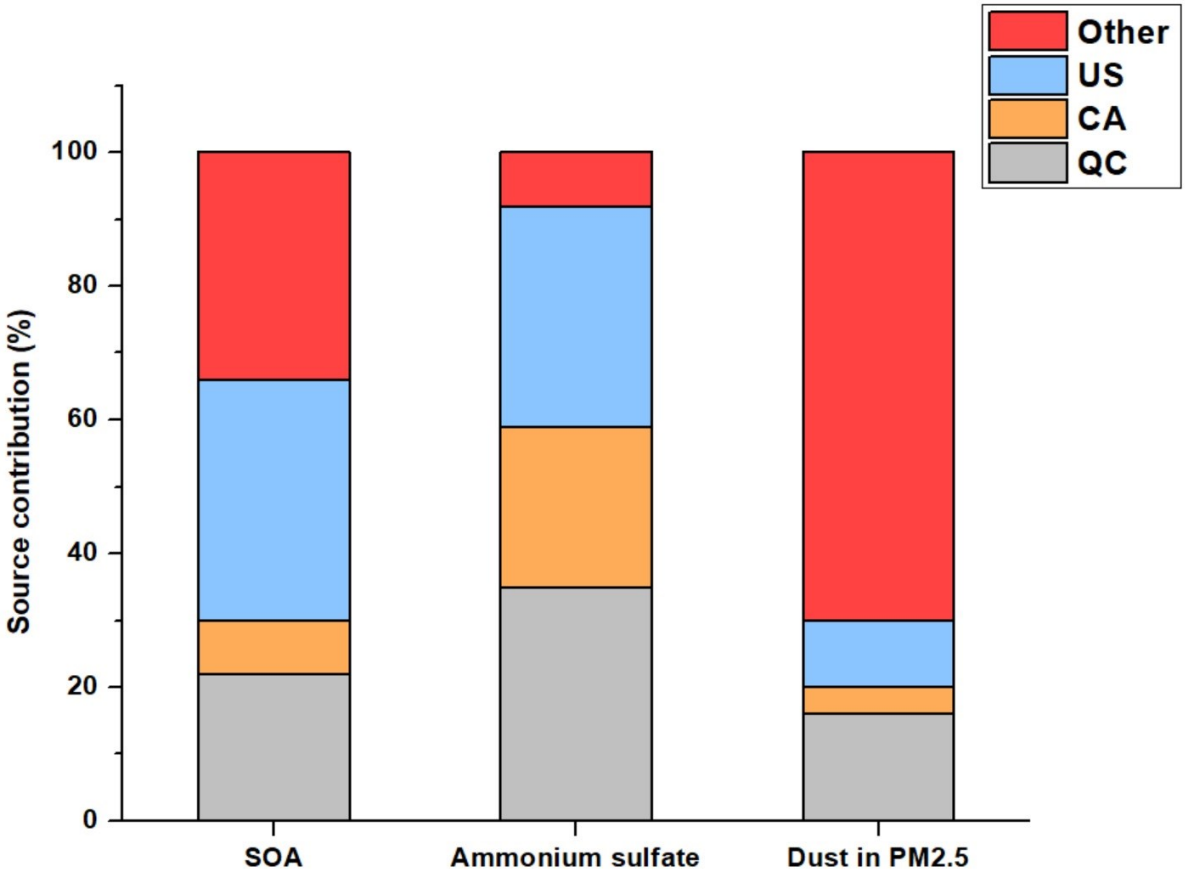

Figure ~~7~~6. Contribution of anthropogenic emissions from three different source regions, namely Qu~~é~~ébec (QC), United States (US) and the rest of Canada (CA) to concentrations of SOA, ammonium sulfate, and dust in $PM_{2.5}$ between August and November 2020, as predicted by GEOS-Chem.

625

3.7 Health risk assessment of $PM_{2.5}$ elements

The non-carcinogenic health risks from airborne elements through inhalation, ingestion and dermal contact were estimated. The HI exhibited the same trend for both children and adults and followed a decreasing order of Co > Mn > Pb > Cu > Cd > Ni > Cr(VI) > Sb > Zn> Al > Fe > V. Among the three exposure pathways, inhalation contributed the most to the total non-
630 carcinogenic risk (HI_{total}). Overall, inhalation contributed 98% for adults and 97% for children to HI_{total}, ingestion contributed 1% (adults) and 2% (children) while dermal absorption was the remainder. Co was the largest contributor to the $HI_{inhalation}$, with a contribution of 61% for both adults and children. An HI value higher than one implies that adverse effects other than cancer such as cardiovascular and respiratory diseases are expected (Fadel et al., 2022a). In this study, HI and HI_{total} (HI_{total} = 0.24 for adults and 0.36 for children) were below the level of 1, highlighting limited non-carcinogenic health hazards from
635 $PM_{2.5}$-metals.

The carcinogenic risk of each carcinogenic metal (i.e., Cr(VI), Co, Ni, V, Cd and Pb) from the three exposures pathways was also calculated. Inhalation was the exposure pathway with the highest cancer risk to which 99% and 98% of the overall carcinogenic risk (CR_{total}) for adults and children was ascribed, respectively. According to the USEPA, a cancer risk value between 10^{-6} (one additional case per one million people) and 10^{-4} (one in a ten thousand) indicates that the carcinogenic risk is considered as tolerable, while a value higher than 10^{-4} indicates that a serious risk of cancer exists (Bari and Kindzierski, 2016; Dahmardeh Behrooz et al., 2021).

In this study, the carcinogenic risk of V, Ni, Cd and Pb was between $1.18x10^{-8}$ and $6.11x10^{-7}$, which is lower than 10^{-6}. However, Co and Cr(VI) presented a cancer risk higher than 10^{-6} (**Fig. ~~8~~7**), highlighting that more attention should be given to these trace metals. Based on PMF analysis, Co was associated with industrial emissions and the correlation between Co and Cr (R=0.79, $p<0.01$) (section 3.4) suggests a common source from industrial emissions for these two trace elements (Cr was not added in the PMF analysis because it was not well modeled). The sum of the risk levels posed by the six metals was 1.77×10^{-5} and 5.87×10^{-6} for adults and children, respectively, which is between the range of 10^{-6} - 10^{-4}, indicating that the carcinogenic risk is considered as tolerable.

These results show that even though industrial emissions presented a very small contribution in term of mass (0.26 µg/m^3), the health risks associated with this source cannot be fully determined by the $PM_{2.5}$ mass concentration alone, and the trace elements emitted from industrial sources source were found to have a potential health risk. Thus, this study highlights that mitigation strategies should also prioritize reduction in metals in addition to PM.

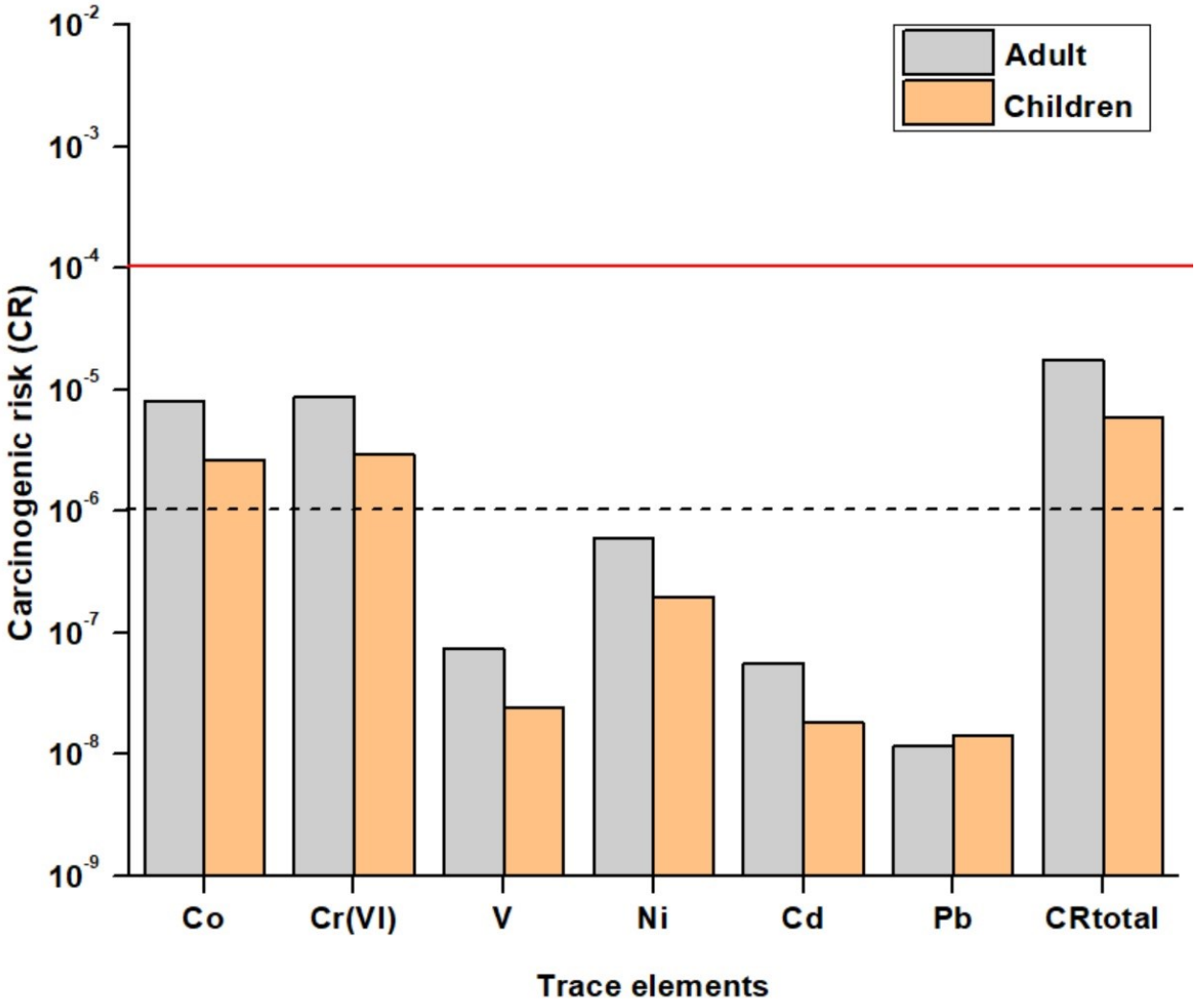

Figure ~~8~~7. The carcinogenic risk (CR_{total}) from trace metals in $PM_{2.5}$. A cancer risk value between 10^{-6} and 10^{-4} indicates that the CR is considered tolerable while a value higher than 10^{-4} indicates that cancer risk exists seriously.

4 Conclusion

This work examines $PM_{2.5}$ sources in Montréal using detailed chemical speciation data collected over a 3-month period (August-November 2020). The chemical composition data included concentrations of the major components such as OC, EC, water-soluble ions, and elements. These species, along with a large suit of organic tracers were used as inputs in a source apportionment model (PMF) to identify and quantify the sources of $PM_{2.5}$. This source apportionment study, which used a wide range of organic molecular markers to investigate the main sources of $PM_{2.5}$, is the first of its kind in Montréal

and Canada. SOA and SIA were major sources and constituted 39% of the measured $PM_{2.5}$ mass. The local primary anthropogenic sources, namely traffic exhaust, road dust, industrial and cooking emissions contributed to 23% of the measured $PM_{2.5}$ mass. These sources along with crustal dust and biomass burning represented the total primary aerosol and accounted altogether for 44% of $PM_{2.5}$. According to the chemical transport model GEOS-Chem, both local (from Québec) and transboundary pollution (from the United States) contribute to the observed concentrations of SOA and SIA in Montréal, but the transboundary contribution is greater than the local contribution, indicating the need to update international agreements to further limit transboundary pollution.

One of the novel aspects of the present study was the inclusion of specific organic tracers which allowed the identification of 4 sources in addition to those that are usually identified using chemical speciation datasets from government monitoring alone. Specifically, these sources (tracers) are plant wax (high MW n-alkanes), BSOA (α-pinene oxidation products), secondary organic aerosols (dicarboxylic acids) and cooking emissions (fatty acids). Moreover, the distinction between exhaust and non-exhaust vehicular emissions was achieved by incorporating two source-specific organic tracers in the PMF model, namely n-alkanes and hopane.

Evaluation of the health risk associated with exposure to metals revealed that Co and Cr(VI) presented a cancer risk (CR) higher than 10^{-6}, highlighting that more attention should be given to these trace metals, which originate principally from industrial emissions according to the PMF analysis. While industrial emissions are the dominant source of Co and Cr(VI), they only contribute a small amount to the total PM2.5 (6%) indicating that the prioritization of sources and sectors for mitigation strategies will be different when considering the concentrations of individual contaminants or total $PM_{2.5}$ concentration.

Data availability: Data used in this study can be accessed here: https://doi.org/10.5683/SP3/96IVPX. More details on the analyses are available upon request to the contact author Nansi Fakhri (nansi.fakhri@umontreal.ca).

Author contributions.

Nansi Fakhri: field campaign and collection of the filters; chemical characterization of the collected filters; analyzing the data and writing the manuscript, **Robin Stevens:** application of GEOS-chem software; review and editing the manuscript, **Arnold Downey:** chemical characterization of the collected filters by ICP-MS, **Konstantina Oikonomou**: resources, **Jean Sciare:** resources, review and editing the manuscript, **Patrick L. Hayes**: supervision, review and editing the manuscript, project administration and resources, **Charbel Afif:** supervision, review and editing the manuscript.

Competing interests. The authors declare that they have no conflict of interest.

Acknowledgement.

PLH and NF acknowledge support from the Natural Science and Engineering Research Council of Canada (NSERC) Discovery Grant Program (RGPIN/05002-0214), Canada Foundation for Innovation Grant (CFI, Leaders Opportunity Fund Projects, grant number 32277) and the Ministère de l'Environnement et de la Lutte contre les changements climatiques (MELCC). NF also acknowledges a scholarship from the *Centre de recherche en écotoxicologie du Québec* (EcotoQ), a strategic cluster funded by the *Fonds de recherche du Québec – Nature et technologies*. This publication has been produced within the framework of the EMME-CARE project, which has received funding from the European Union Horizon 2020 Research and Innovation Program (under grant agreement no. 856612) and the Cyprus Government. The research was also enabled in part by support provided by Calcul Québec (calculquebec.ca) and the Digital Research Alliance of Canada (alliancecan.ca). This work contains modified Copernicus Atmosphere Monitoring Service Information [2020]. Neither the European Commission nor ECMWF is responsible for any use that may be made of the information it contains.

References

Abdallah, C., Afif, C., El Masri, N., Öztürk, F., Keleş, M., Sartelet, K. A first annual assessment of air quality modeling over Lebanon using WRF/Polyphemus. Atmos. Pollut. Res. 9, 643–654. https://doi.org/10.1016/j.apr.2018.01.003, 2018.

Bari, M.A., Kindzierski, W.B. Fine particulate matter ($PM_{2.5}$) in Edmonton, Canada: Source apportionment and potential risk for human health. Environ. Pollut. 218, 219–229. https://doi.org/10.1016/j.envpol.2016.06.014, 2016.

Belis, C., Larsen, B. R., Amato, F., Haddad, I. El, Favez, O., Harrison, R. M., Hopke, P. K., Nava, S., Paatero, P., Prévôt, A., Quass, U., Vecchi, R., Viana, M. European Guide on Air Pollution Source Apportionment with Receptor Models. JRC References Report, March, 88. https://doi.org/10.2788/9307, 2019.

Bey, I., Jacob, D.J., Yantosca, R.M., Logan, J.A., Field, B.D., Fiore, A.M., Li, Q., Liu, H.Y., Mickley, L.J., Schultz, M.G. Global modeling of tropospheric chemistry with assimilated meteorology: Model description and evaluation. J. Geophys. Res. Atmos. 106, 23073–23095. https://doi.org/10.1029/2001JD000807, 2001.

Cavalli, F., Viana, M., Yttri, K. E., Genberg, J., Putaud, J.P. Toward a standardised thermal-optical protocol for measuring atmospheric organic and elemental carbon: the EUSAAR protocol. Atmos. Meas. Tech., 3, 79–89, https://doi.org/10.5194/amt-3-79-2010, 2010.

Calvo, A.I., Pont, V., Liousse, C., Dupré, B., Mariscal, A., Zouiten, C., Gardrat, E., Castera, P., Lacaux, C.G., Castro, A., Fraile, R. Chemical composition of urban aerosols in Toulouse, France during CAPITOUL experiment. Meteorol. Atmos. Phys. 102, 307–323. https://doi.org/10.1007/s00703-008-0319-2, 2008.

Celo, V., Yassine, M.M., Dabek-Zlotorzynska, E. Insights into elemental composition and sources of fine and coarse particulate matter in dense traffic areas in Toronto and Vancouver, Canada. Toxics 9. https://doi.org/10.3390/toxics9100264, 2021.

Chow, J.C., Lowenthal, D.H., Chen, L.W.A., Wang, X., Watson, J.G. Mass reconstruction methods for $PM_{2.5}$: a review. Air Qual. Atmos. Heal. 8, 243–263. https://doi.org/10.1007/s11869-015-0338-3, 2015.

Dabek-Zlotorzynska, E., Dann, T.F., Kalyani Martinelango, P., Celo, V., Brook, J.R., Mathieu, D., Ding, L., Austin, C.C. Canadian National Air Pollution Surveillance (NAPS) $PM_{2.5}$ speciation program: Methodology and $PM_{2.5}$ chemical composition for the years 2003-2008. Atmos. Environ. 45, 673–686. https://doi.org/10.1016/j.atmosenv.2010.10.024, 2011.

Dahmardeh Behrooz, R., Kaskaoutis, D.G., Grivas, G., Mihalopoulos, N. Human health risk assessment for toxic elements in the extreme ambient dust conditions observed in Sistan, Iran. Chemosphere 262, 127835. https://doi.org/10.1016/j.chemosphere.2020.127835, 2021.

Environmental Assessment Report (EAR) 2017, Air Quality in Montréal, Ville de Montréal Service de l'environnement, Division de la planification et du suivi environnemental, 1–6, 2017.

Environmental Assessment Report (EAR) 2018, Air Quality in Montréal, Ville de Montréal Service de l'environnement, Division de la planification et du suivi environnemental, 1–6, 2018.

Environmental Assessment Report (EAR) 2019, Air Quality in Montréal, Ville de Montréal Service de l'environnement, Division de la planification et du suivi environnemental, 1–16, 2019.

Environmental Assessment Report (EAR) 2020, Air Quality in Montréal, Ville de Montréal Service de l'environnement, Division de la planification et du suivi environnemental, 1–19, 2020.

El Haddad, I., Marchand, N., Dron, J., Temime-Roussel, B., Quivet, E., Wortham, H., Jaffrezo, J.L., Baduel, C., Voisin, D., Besombes, J.L., Gille, G. Comprehensive primary particulate organic characterization of vehicular exhaust emissions in France. Atmos. Environ. 43, 6190–6198. https://doi.org/10.1016/j.atmosenv.2009.09.001, 2009.

El Haddad, I., Marchand, N., Temime-Roussel, B., Wortham, H., Piot, C., Besombes, J.L., Baduel, C., Voisin, D., Armengaud, A., Jaffrezo, J.L. Insights into the secondary fraction of the organic aerosol in a Mediterranean urban area: Marseille. Atmos. Chem. Phys. 11, 2059–2079. https://doi.org/10.5194/acp-11-2059-2011, 2011.

Environmental Protection Agency (EPA) 2021. Accessed September 10, 2021. https://www.epa.gov/air-emissions-modeling/2016v1-platform, 2021a.

Environmental Protection Agency (EPA) Air Pollutant Emissions Trends Data. Accessed September 21, 2021. https://www.epa.gov/air-emissions-inventories/air-pollutant-emissions-trends-data, 2021b.

Esmaeilirad, S., Lai, A., Abbaszade, G., Schnelle-Kreis, J., Zimmermann, R., Uzu, G., Daellenbach, K., Canonaco, F., Hassankhany, H., Arhami, M., Baltensperger, U., Prévôt, A.S.H., Schauer, J.J., Jaffrezo, J.L., Hosseini, V., El Haddad, I. Source apportionment of fine particulate matter in a Middle Eastern Metropolis, Tehran-Iran, using PMF with organic and inorganic markers. Sci. Total Environ. 705, 135330. https://doi.org/10.1016/j.scitotenv.2019.135330, 2020.

Fadel, M., Courcot, D., Afif, C., Ledoux, F. Methods for the assessment of health risk induced by contaminants in atmospheric particulate matter: a review. Environ. Chem. Lett. https://doi.org/10.1007/s10311-022-01461-6, 2022a.

Fadel, M., Ledoux, F., Afif, C., Courcot, D. Human health risk assessment for PAHs, phthalates, elements, PCDD/Fs, and DL-PCBs in $PM_{2.5}$ and for NMVOCs in two East-Mediterranean urban sites under industrial influence. Atmos. Pollut. Res. 13, 101261. https://doi.org/10.1016/j.apr.2021.101261, 2022b.

Fadel, Marc, Ledoux, F., Farhat, M., Kfoury, A., Courcot, D., Afif, C. $PM_{2.5}$ characterization of primary and secondary organic aerosols in two urban-industrial areas in the East Mediterranean. J. Environ. Sci. (China) 101, 98–116. https://doi.org/10.1016/j.jes.2020.07.030, 2021.

Fadel, M., Courcot, D., Seigneur, M., Kfoury, A., Oikonomou, K., Sciare, J., Afif, C. Identification and apportionment of local and long-range sources of $PM_{2.5}$ in two East-Mediterranean sites. Atmos. Pollut. Res. 14, 101622. https://doi.org/10.1016/j.apr.2022.101622, 2023.

Fairlie, T.D., Jacob, D.J., Dibb, J.E., Alexander, B., Avery, M.A., van Donkelaar, A., Zhang, L. Impact of mineral dust on nitrate, sulfate, and ozone in transpacific Asian pollution plumes. Atmospheric Chemistry and Physics 10, 3999–4012. https://doi.org/10.5194/acp-10-3999-2010, 2010.

Fakhri, N., Fadel, M., Öztürk, F., Keleş, M., Iakovides, M., Pikridas, M., Abdallah, C., Karam, C., Sciare, J., Hayes, P.L., Afif, C. Comprehensive chemical characterization of $PM_{2.5}$ in the large East Mediterranean-Middle East city of Beirut, Lebanon. J. Environ. Sci. 133, 118–137. https://doi.org/10.1016/j.jes.2022.07.010, 2023.

Gadi, R., Shivani, Sharma, S.K., Mandal, T.K. Source apportionment and health risk assessment of organic constituents in fine ambient aerosols ($PM_{2.5}$): A complete year study over National Capital Region of India. Chemosphere 221, 583–596. https://doi.org/10.1016/j.chemosphere.2019.01.067, 2019.

Genga, A., Ielpo, P., Siciliano, T., Siciliano, M. Carbonaceous particles and aerosol mass closure in $PM_{2.5}$ collected in a port city. Atmos. Res. 183, 245–254. https://doi.org/10.1016/j.atmosres.2016.08.022, 2017.

Government of Québec. Impact of COVID-19 on air quality in Québec. https://www.quebec.ca/en/agriculture-environment-and-natural-resources/environment-covid-19/impact-air-quality-quebec-covid-19 (accessed 26 September 2022), 2022.

Hallquist, M., Wenger, J.C., Baltensperger, U., Rudich, Y., Simpson, D., Claeys, M., Dommen, J., Donahue, N.M., George, C., Goldstein, A.H., Hamilton, J.F., Herrmann, H., Hoffmann, T., Iinuma, Y., Jang, M., Jenkin, M.E., Jimenez, J.L., Kiendler-Scharr, A., Maenhaut, W., McFiggans, G., Mentel, T.F., Monod, A., Prévôt, A.S.H., Seinfeld, J.H., Surratt, J.D., Szmigielski, R., Wildt, J. The formation, properties and impact of secondary organic aerosol: Current and emerging issues. Atmos. Chem. Phys. 9, 5155–5236. https://doi.org/10.5194/acp-9-5155-2009, 2009.

Hao, Y., Luo, B., Simayi, M., Zhang, W., Jiang, Y., He, J., Xie, S. Spatiotemporal patterns of $PM_{2.5}$ elemental composition over China and associated health risks. Environ. Pollut. 265, 114910. https://doi.org/10.1016/j.envpol.2020.114910, 2020.

Health Canada. Health Impacts of Air Pollution in Canada, Estimates of Premature Deaths and Nonfatal Outcomes, 2021 Report, 1–56, 2021.

Huang, X.H.H., Bian, Q., Ng, W.M., Louie, P.K.K., Yu, J.Z. Characterization of $PM_{2.5}$ major components and source investigation in suburban Hong Kong: A one year monitoring study. Aerosol Air Qual. Res. 14, 237–250, doi: 10.4209/aaqr.2013.01.0020, 2014.

Hoesly, R.M., Smith, S.J., Feng, L., Klimont, Z., Janssens-Maenhout, G., Pitkanen, T., Seibert, J.J., Vu, L., Andres, R.J., Bolt, R.M., Bond, T.C., Dawidowski, L., Kholod, N., Kurokawa, J.I., Li, M., Liu, L., Lu, Z., Moura, M.C.P., O'Rourke, P.R., Zhang, Q. Historical (1750-2014) anthropogenic emissions of reactive gases and aerosols from the Community Emissions Data System (CEDS). Geosci. Model Dev. 11, 369–408. https://doi.org/10.5194/gmd-11-369-2018, 2018.

Jeong, C.H., McGuire, M.L., Herod, D., Dann, T., Dabek-Zlotorzynska, E., Wang, D., Ding, L., Celo, V., Mathieu, D., Evans, G. Receptor model-based identification of $PM_{2.5}$ sources in Canadian cities. Atmos. Pollut. Res. 2, 158–171. https://doi.org/10.5094/APR.2011.021, 2011.

Joseph, A.E., Unnikrishnan, S., Kumar, R. Chemical characterization and mass closure of fine aerosol for different land use patterns in Mumbai city. Aerosol Air Qual. Res. 12, 61–72. https://doi.org/10.4209/aaqr.2011.04.0049, 2012.

Kaiser, J. W., Heil, A., Andreae, M. O., Benedetti, A., Chubarova, N., Jones, L., Morcrette, J.-J., Razinger, M., Schultz, M. G., Suttie, M., and van der Werf, G. R.: Biomass burning emissions estimated with a global fire assimilation system based on observed fire radiative power, Biogeosciences, 9, 527–554, https://doi.org/10.5194/bg-9-527-2012, 2012.

Keller, C. A., Long, M. S., Yantosca, R. M., Da Silva, A. M., Pawson, S., Jacob, D. J., 2014. HEMCO v1.0: a versatile, ESMF-compliant component for calculating emissions in atmospheric models, Geosci. Model Dev., 7, 1409–1417, https://doi.org/10.5194/gmd-7-1409-2014.

Khan, J.Z., Sun, L., Tian, Y., Shi, G., Feng, Y. Chemical characterization and source apportionment of PM_1 and $PM_{2.5}$ in Tianjin, China: Impacts of biomass burning and primary biogenic sources. J. Environ. Sci. (China) 99, 196–209. https://doi.org/10.1016/j.jes.2020.06.027, 2021.

Kim, P.S., Jacob, D.J., Fisher, J.A., Travis, K., Yu, K., Zhu, L., Yantosca, R.M., Sulprizio, M.P., Jimenez, J.L., Campuzano-Jost, P., Froyd, K.D., Liao, J., Hair, J.W., Fenn, M.A., Butler, C.F., Wagner, N.L., Gordon, T.D., Welti, A., Wennberg, P.O., Crounse, J.D., St. Clair, J.M., Teng, A.P., Millet, D.B., Schwarz, J.P., Markovic, M.Z., Perring, A.E. Sources, seasonality, and trends of southeast US

aerosol: an integrated analysis of surface, aircraft, and satellite observations with the GEOS-Chem chemical transport model. Atmos. Chem. Phys. 15, 10411–10433. https://doi.org/10.5194/acp-15-10411-2015, 2015.

Lelieveld, J., Klingmüller, K., Pozzer, A., Pöschl, U., Fnais, M., Daiber, A., Münzel, T. Cardiovascular disease burden from ambient air pollution in Europe reassessed using novel hazard ratio functions. Eur. Heart J. 40, 1590–1596. https://doi.org/10.1093/eurheartj/ehz135, 2019.

Lee, Y.S., Kim, Y.K., Choi, E., Jo, H., Hyun, H., Yi, S.M., Kim, J.Y. Health risk assessment and source apportionment of $PM_{2.5}$-bound toxic elements in the industrial city of Siheung, Korea. Environ. Sci. Pollut. Res. 29, 66591–66604, https://doi.org/10.1007/s11356-022-20462-0, 2022.

Lin, Y.C., Tsai, C.J., Wu, Y.C., Zhang, R., Chi, K.H., Huang, Y.T., Lin, S.H., Hsu, S.C. Characteristics of trace metals in traffic-derived particles in Hsuehshan Tunnel, Taiwan: Size distribution, potential source, and fingerprinting metal ratio. Atmos. Chem. Phys. 15, 4117–4130. https://doi.org/10.5194/acp-15-4117-2015, 2015.

Luo, G., Yu, F., and Schwab, J.: Revised treatment of wet scavenging processes dramatically improves GEOS-Chem 12.0.0 simulations of surface nitric acid, nitrate, and ammonium over the United States, Geosci. Model Dev., 12, 3439–3447, https://doi.org/10.5194/gmd-12-3439-2019, 2019.

Luo, G., Yu, F., and Moch, J. M.: Further improvement of wet process treatments in GEOS-Chem v12.6.0: impact on global distributions of aerosols and aerosol precursors, Geosci. Model Dev., 13, 2879–2903, https://doi.org/10.5194/gmd-13-2879-2020, 2020.

Lv, L., Chen, Y., Han, Y., Cui, M., Wei, P., Zheng, M., Hu, J. High-time-resolution $PM_{2.5}$ source apportionment based on multi-model with organic tracers in Beijing during haze episodes. Sci. Total Environ. 772, 144766. https://doi.org/10.1016/j.scitotenv.2020.144766, 2021.

Mason, B., & Moore, C.B. Principles of Geochemistry, fourth edition. Wiley. 1982.

Mancilla, Y., Mendoza, A. A tunnel study to characterize $PM_{2.5}$ emissions from gasoline-powered vehicles in Monterrey, Mexico. Atmos. Environ. 59, 449–460. https://doi.org/10.1016/j.atmosenv.2012.05.025, 2012.

Meng, J., Martin, R. V., Li, C., van Donkelaar, A., Tzompa-Sosa, Z. A., Yue, X., Xu, J.-W., Weagle, C. L., and Burnett, R. T.: Source Contributions to Ambient Fine Particulate Matter for Canada, Environ. Sci. Technol., 53, 10269–10278, https://doi.org/10.1021/acs.est.9b02461, 2019.

Nansai, K., Tohno, S., Chatani, S., Kanemoto, K., Kagawa, S., Kondo, Y., Takayanagi, W., Lenzen, M. Consumption in the G20 nations causes particulate air pollution resulting in two million premature deaths annually. Nat. Commun. 12, 1–6. https://doi.org/10.1038/s41467-021-26348-y, 2021.

NPRID. National Pollutant Release Inventory Dashboard, Government of Canada. Accessed August 30, 2022. https://www.canada.ca/en/environment-climate-change/services/national-pollutant-release-inventory/tools-resources-data/all-year-dashboard.html, 2022.

O'Rourke, P., Smith, S., Mott, A., Ahsan, H., Mcduffie, E., Crippa, M., Klimont, Z., Mcdonald, B., Wang, S., Nicholson, M., Hoesly, R., and Feng, L.: CEDS v_2021_04_21 Gridded emissions data, https://doi.org/10.25584/PNNLDATAHUB/1779095, 2021.

Pant, P., Harrison, R.M. Estimation of the contribution of road traffic emissions to particulate matter concentrations from field measurements: A review. Atmos. Environ. 77, 78–97. https://doi.org/10.1016/j.atmosenv.2013.04.028, 2013.

Park, R.J., Jacob, D.J., Field, B.D., Yantosca, R.M., Chin, M. Natural and transboundary pollution influences on sulfate-nitrate-ammonium aerosols in the United States: Implications for policy. J. Geophys. Res. 109. https://doi.org/10.1029/2003jd004473, 2004.

Park, M-B., Lee, T.J., Lee, E.S., Kim, D.S. Enhancing source identification of hourly $PM_{2.5}$ data in Seoul based on a dataset segmentation scheme by positive matrix factorization (PMF). Atmos. Pollut. Res. 10, 1042–1059. https://doi.org/10.1016/j.apr.2019.01.013, 2019.

Pai, S.J., Heald, C.L., Pierce, J.R., Farina, S.C., Marais, E.A., Jimenez, J.L., Campuzano-Jost, P., Nault, B.A., Middlebrook, A.M., Coe, H., Shilling, J.E., Bahreini, R., Dingle, J.H., Vu, K. An evaluation of global organic aerosol schemes using airborne observations. Atmos. Chem. Phys. 20, 2637–2665. https://doi.org/10.5194/acp-20-2637-2020, 2020.

Petit, J.E., Pallarès, C., Favez, O., Alleman, L.Y., Bonnaire, N., Rivière, E. Sources and geographical origins of PM10 in Metz (France) using oxalate as a marker of secondary organic aerosols by positive matrix factorization analysis. Atmosphere (Basel). 10. https://doi.org/10.3390/atmos10070370, 2019.

Philip, S., Martin, R. V., Snider, G., Weagle, C. L., van Donkelaar, A., Brauer, M., Henze, D. K., Klimont, Z., Venkataraman, C., Guttikunda, S. K., and Zhang, Q., 2017. Anthropogenic fugitive, combustion and industrial dust is a significant, underrepresented fine particulate matter source in global atmospheric models, Environ. Res. Lett., 12, 044018, https://doi.org/10.1088/1748-9326/aa65a4, 2017.

Pio, C., Mirante, F., Oliveira, César, Matos, M., Caseiro, A., Oliveira, Cristina, Querol, X., Alves, C., Martins, N., Cerqueira, M., Camões, F., Silva, H., Plana, F. Size-segregated chemical composition of aerosol emissions in an urban road tunnel in Portugal. Atmos. Environ. 71, 15–25. https://doi.org/10.1016/j.atmosenv.2013.01.037, 2013.

Polissar, A. V., Hopke, P.K., Paatero, P., Malm, W.C., Sisler, J.F. Atmospheric aerosol over Alaska. 2. Elemental composition and sources. J. Geophys. Res. Atmos. 103. 1998.

Rahn, K.A., Huang, S. A graphical technique for distinguishing soil and atmospheric deposition in biomonitors from the plant material. Sci. Total Environ. 232, 79–104. https://doi.org/10.1016/S0048-9697(99)00112-6, 1999.

Reidmiller, D.R., Fiore, A.M., Jaffe, D.A., Bergmann, D., Cuvelier, C., Dentener, F.J., Duncan, B.N., Folberth, G., Gauss, M., Gong, S., Hess, P., Jonson, J.E., Keating, T., Lupu, A., Marmer, E., Park, R., Schultz, M.G., Shindell, D.T., Szopa, S., Vivanco, M.G., Wild, O., Zuber, A. The influence of foreign vs. North American emissions on surface ozone in the US. Atmos. Chem. Phys. 9, 5027–5042. https://doi.org/10.5194/acp-9-5027-2009, 2009.

Riffault, V., Arndt, J., Marris, H., Mbengue, S., Setyan, A., Alleman, L.Y., Deboudt, K., Flament, P., Augustin, P., Delbarre, H., Wenger, J. Fine and ultrafine particles in the vicinity of industrial activities: A review. Crit. Rev. Environ. Sci. Technol. 45, 2305–2356. https://doi.org/10.1080/10643389.2015.1025636, 2015.

Rogge, W.F., Hildemann, L.M., Mazurek, M.A., Cass, G.R., Simoneit, B.R.T. Sources of Fine Organic Aerosol. 2. Noncatalyst and Catalyst-Equipped Automobiles and Heavy-Duty Diesel Trucks. Environ. Sci. Technol. 27, 636–651. https://doi.org/10.1021/es00041a007, 1993a.

Rogge, W.F., Hildemann, L.M., Mazurek, M.A., Cass, G.R., Simonelt, B.R.T. Sources of Fine Organic Aerosol. 4. Particulate Abrasion Products from Leaf Surfaces of Urban Plants. Environ. Sci. Technol. 27, 2700–2711. https://doi.org/10.1021/es00049a008, 1993b.

Roy, D., Singh, G., Seo, Y. Carcinogenic and non-carcinogenic risks from PM_{10} -and $PM_{2.5}$ -Bound metals in a critically polluted coal mining area. Atmos. Pollut. Res. 10, 1964–1975. https://doi.org/10.1016/j.apr.2019.09.002, 2019.

Salameh, D., Detournay, A., Pey, J., Pérez, N., Liguori, F., Saraga, D., Bove, M.C., Brotto, P., Cassola, F., Massabò, D., Latella, A., Pillon, S., Formenton, G., Patti, S., Armengaud, A., Piga, D., Jaffrezo, J.L., Bartzis, J., Tolis, E., Prati, P., Querol, X., Wortham, H., Marchand, N. $PM_{2.5}$ chemical composition in five European Mediterranean cities: A 1-year study. Atmos. Res. 155, 102–117. https://doi.org/10.1016/j.atmosres.2014.12.001, 2015.

Seinfeld, J.H. and Pandis, S.N. Atmospheric Chemistry and Physics: From air pollution to climate change, 1360 pp., John Wiley and Sons, New York, 2016.

Schauer, J.J., Kleeman, M.J., Cass, G.R., Simoneit, B.R.T. Measurement of emissions from air pollution sources. 5. C1 - C32 organic compounds from gasoline-powered motor vehicles. Environ. Sci. Technol. 36, 1169–1180. https://doi.org/10.1021/es0108077, 2002.

Sciare, J., Oikonomou, K., Cachier, H., Mihalopoulos, N., Andreae, M.O., Maenhaut, W., et al. Aerosol mass closure and reconstruction of the light scattering coefficient over the Eastern Mediterranean Sea during the MINOS campaign. Atmos. Chem. Phys. Discuss. 5, 2427–2461, doi:10.5194/acp-5-2253-2005, 2005.

Simone, N.W., Stettler, M.E.J., Barrett, S.R.H. Rapid estimation of global civil aviation emissions with uncertainty quantification. Transp. Res. Part D Transp. Environ. 25, 33–41. https://doi.org/10.1016/j.trd.2013.07.001, 2013.

Sharma, S.K., Mandal, T.K. Chemical composition of fine mode particulate matter ($PM_{2.5}$) in an urban area of Delhi, India and its source apportionment. Urban Clim. 21, 106–122. https://doi.org/10.1016/j.uclim.2017.05.009, 2017.

Shivani, Gadi, R., Sharma, S.K., Mandal, T.K. Seasonal variation, source apportionment and source attributed health risk of fine carbonaceous aerosols over National Capital Region, India. Chemosphere 237, 124500. https://doi.org/10.1016/j.chemosphere.2019.124500, 2019.

Silvern, R.F., Jacob, D.J., Mickley, L.J., Sulprizio, M.P., Travis, K.R., Marais, E.A., Cohen, R.C., Laughner, J.L., Choi, S., Joiner, J., Lamsal, L.N., 2019. Using satellite observations of tropospheric NO_2; columns to infer long-term trends in US NOx emissions: the importance of accounting for the free tropospheric NO_2 background. Atmos. Chem. Phys. 19, 8863–8878. https://doi.org/10.5194/acp-19-8863-2019, 2019.

Simoneit, B.R.T. Biomass burning - A review of organic tracers for smoke from incomplete combustion, Applied Geochemistry. https://doi.org/10.1016/S0883-2927(01)00061-0, 2002.

Srivastava, D., Favez, O., Petit, J.E., Zhang, Y., Sofowote, U.M., Hopke, P.K., Bonnaire, N., Perraudin, E., Gros, V., Villenave, E., Albinet, A. Speciation of organic fractions does matter for aerosol source apportionment. Part 3: Combining off-line and on-line measurements. Sci. Total Environ. 690, 944–955. https://doi.org/10.1016/j.scitotenv.2019.06.378, 2019.

Stettler, M.E.J., Eastham, S., Barrett, S.R.H. Air quality and public health impacts of UK airports. Part I: Emissions. Atmos. Environ. 45, 5415–5424. https://doi.org/10.1016/j.atmosenv.2011.07.012, 2011.

Thorpe, A., Harrison, R.M. Sources and properties of non-exhaust particulate matter from road traffic: A review. Sci. Total Environ. 400, 270–282. https://doi.org/10.1016/j.scitotenv.2008.06.007, 2008.

USATODAY. COVID-19 restrictions, Map of COVID-19 case trends and restrictions, https://www.usatoday.com/storytelling/coronavirus-reopening-america-map/ (accessed 27 September 2022), 2022.

USEPA. Users' guide and background technical document for US EPA region 9's preliminary remediation goals (PRG) table. 1–30, 2004.

USEPA. Exposure Factors Handbook: 2011 Edition. National Center for Environmental Assessment, Washington, DC; EPA/600/R-09/052F. Available from the National Technical Information Service, Springfield, VA, and online at http://www.epa.gov/ncea/efh, 2011.

USEPA. EPA Positive Matrix Factorization (PMF) 5.0 Fundamentals and User Guide. U.S. Environmental Protection Agency Office of Research and Development Washington, DC 20460, 2014.

WHO. WHO global air quality guidelines: particulate matter ($PM_{2.5}$ and PM_{10}), ozone, nitrogen dioxide, sulfur dioxide and carbon monoxide. Geneva: World Health Organization; 2021. https://apps.who.int/iris/handle/10665/345329 (accessed 27 July 2022), 2021.

Zender, C. S. 2003. Mineral Dust Entrainment and Deposition (DEAD) model: Description and 1990s dust climatology, J. Geophys. Res., 108, 4416, https://doi.org/10.1029/2002JD002775, 2003.

Zhang, L., Kok, J.F., Henze, D.K., Li, Q., Zhao, C. Improving simulations of fine dust surface concentrations over the western United States by optimizing the particle size distribution. Geophys. Res. Lett. 40, 3270–3275. https://doi.org/10.1002/grl.50591, 2013.

SUPPLEMENTARY INFORMATION

Source Apportionment of $PM_{2.5}$ in Montréal, Canada and Health Risk Assessment for Potentially Toxic Elements

Nansi Fakhri [a,b], Robin Stevens [b], Arnold Downey [b], Konstantina Oikonomou [c], Jean Sciare [c], Charbel Afif* [a,c], Patrick L. Hayes* [b]

[a] EMMA Research Group, Centre d'Analyses et de Recherche, Faculty of Sciences, Université Saint-Joseph, Beirut, Lebanon

[b] Department of Chemistry, Faculty of Arts and Sciences, Université de Montréal, Montréal, Québec, Canada

[c] Climate and Atmosphere Research Center (CARE-C), The Cyprus Institute, Nicosia, Cyprus

Table S1: Values of the cancer slope factor (CSF) and inhalation unit risk (IUR).

	Cancer slope factor (CSF) (kg·day/mg)			Inhalation unit risk (IUR) (m^3/mg)
	Dermal	**Ingestion**	**Inhalation**	
Co			9.8	9
Cr(VI)	20	0.5	41	84
Ni			0.84	0.26
V				8.3
Cd			6.3	1.8
Pb	0.0085	0.0085	0.042	0.000012

Table S2: Displacement error estimation and mapping of bootstrap factors to constrained factors for the PMF model.

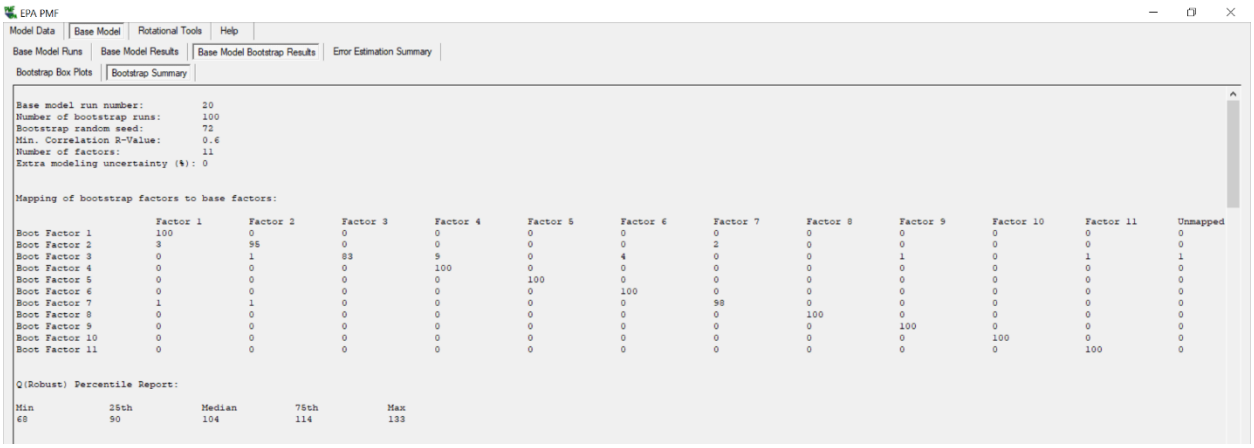

In order to reduce the range of the meaningful number of factors, two parameters was calculated: the maximum individual mean (IM) and the maximum individual standard deviation (IS) where (Lee et al., 1999):

$$IM = \max_{j=1\ldots m}\left(\frac{1}{n}\sum_{i=1}^{n} r_{ij}\right) \quad \text{and} \quad IS = \max_{j=1\ldots m}\left(\sqrt{\frac{1}{n-1}\sum_{i=1}^{n}(r_{ij} - \bar{r}_j)^2}\right)$$

$$r_{ij} = \frac{e_{ij}}{s_{ij}}$$

When the number of factors increases to a critical value, IM and IS will show a drastic drop.

Graphical representations of the IM and IS (**Fig. S1**) revealed a steady drop in their values as the number of factors increased and a stabilization starting with the 11-factor solution. Moreover, a 12-factor solution resolved a phantom factor that could not be definitively linked to a particular source, while a 10-factor solution consolidated two sources into a single factor (Esmaeilirad et al., 2020).

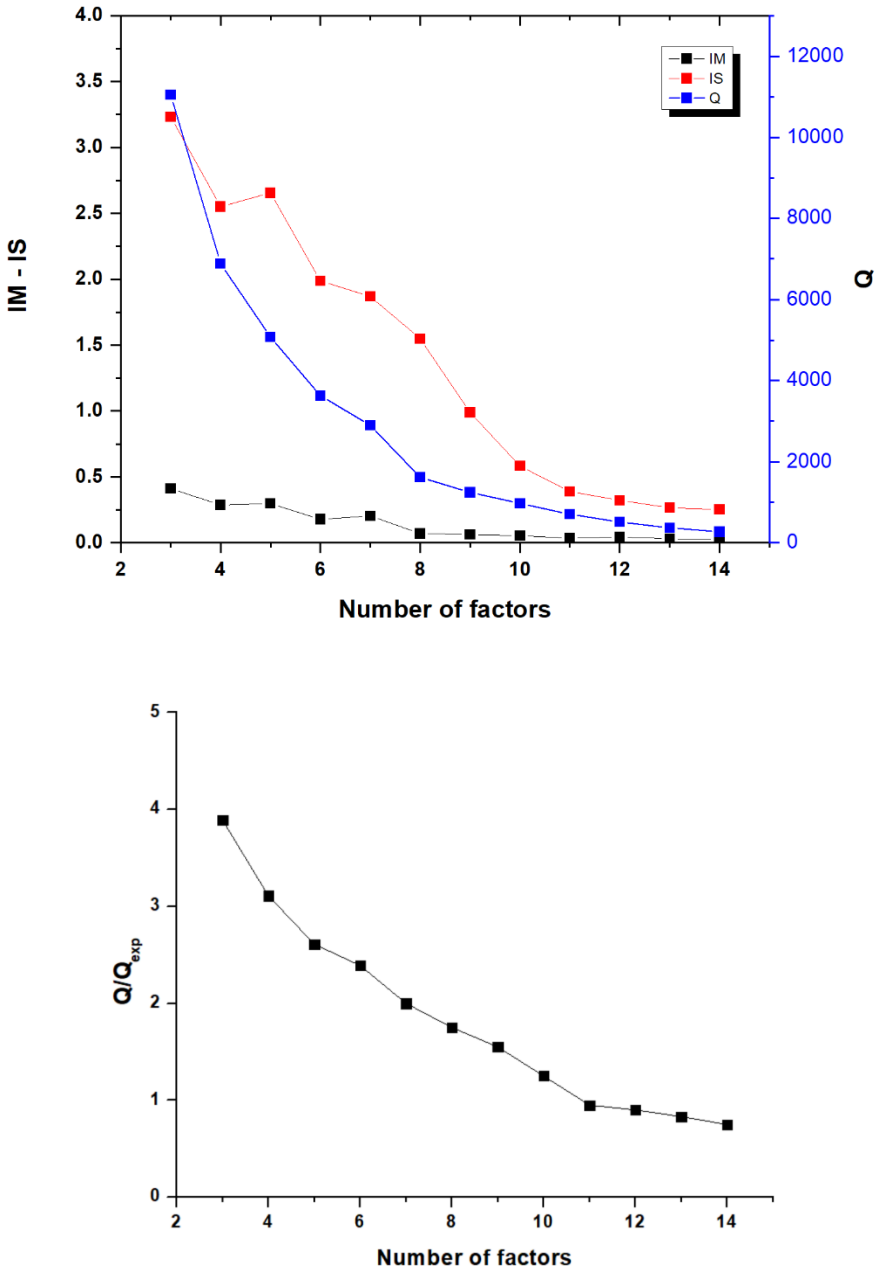

Fig. S1: IM, IS and Q-values for MTL site.

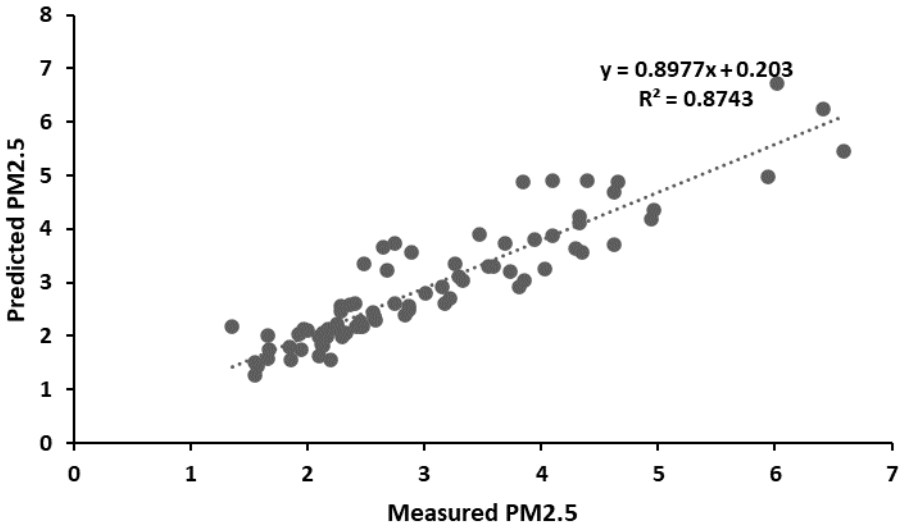

Fig. S2: Measured versus predicted $PM_{2.5}$ concentrations.

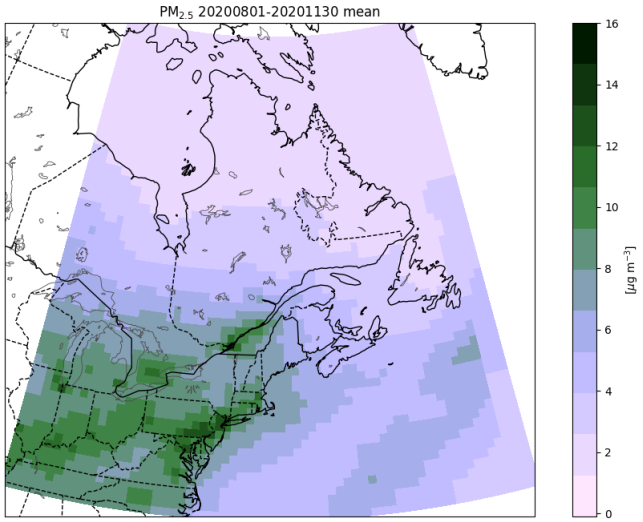

Fig. S3: Mean concentrations of $PM_{2.5}$ from the base case 0.5x0.625 nested GEOS-Chem simulation.

Evaluation of GEOS-Chem against measurements

The model performance was evaluated for $PM_{2.5}$, SO_4^{2-}, NO_3^-, NH_4^+, OC and EC and the results are summarized in **Table S3**. The metrics used for the evaluation were: Pearson's correlation coefficient (R), mean error (ME), normalized mean error (NME), mean bias (MB), and normalized mean bias (NMB). ME, NME, MB, and NMB are calculated following the Eqs. 1-4, where x_i indicates the model predictions and y_i indicates the observed data for a given month and station, both as daily averages, and N is the number of model-observation pairs:

$$ME = \frac{1}{N}\sum_{i=1}^{N}|x_i - y_i| \qquad \text{(Eq. 1)}$$

$$NME = \frac{1}{N}\sum_{i=1}^{N}\frac{|x_i - y_i|}{y_i}\cdot 100 \qquad \text{(Eq. 2)}$$

$$MB = \frac{1}{N}\sum_{i=1}^{N} x_i - y_i \qquad \text{(Eq. 3)}$$

$$NMB = \frac{1}{N}\sum_{i=1}^{N}\frac{(x_i - y_i)}{y_i}\cdot 100 \qquad \text{(Eq. 4)}$$

Table S3: Evaluation of the GEOS-Chem base case simulation vs measurements from our measurement site.

Pollutants	**R**	**ME**	**NME [%]**	**MB**	**NMB [%]**
$PM_{2.5}$ (μg m^{-3})	0.63	4.69	141.08	4.46	133.98
SO_4^{2-} (μg m^{-3})	0.24	0.43	77.14	0.18	32.39
NO_3^- (μg m^{-3})	0.56	0.30	107.92	0.11	40.95
NH_4^+(μg m^{-3})	0.46	0.23	89.09	0.15	57.08
OC (μg m^{-3})	0.76	0.89	51.46	0.11	41.02
EC (μg m^{-3})	0.57	0.16	58.84	0.01	2.89

We note that significant errors are expected due to the differences in spatial extent of the model resolution (0.5 degrees latitude by 0.625 degrees longitude) versus the observations (essentially a point measurement) as discussed by Schutgens et al. (2016). However, this bias is expected to affect all of the sensitivity simulations in a similar way and would not affect the relative differences between simulations that we use to help interpret the results of the PMF analysis. Furthermore, GEOS-Chem results have been previously used for source contribution analysis similar to the analysis presented in this study (Meng et al. 2019).

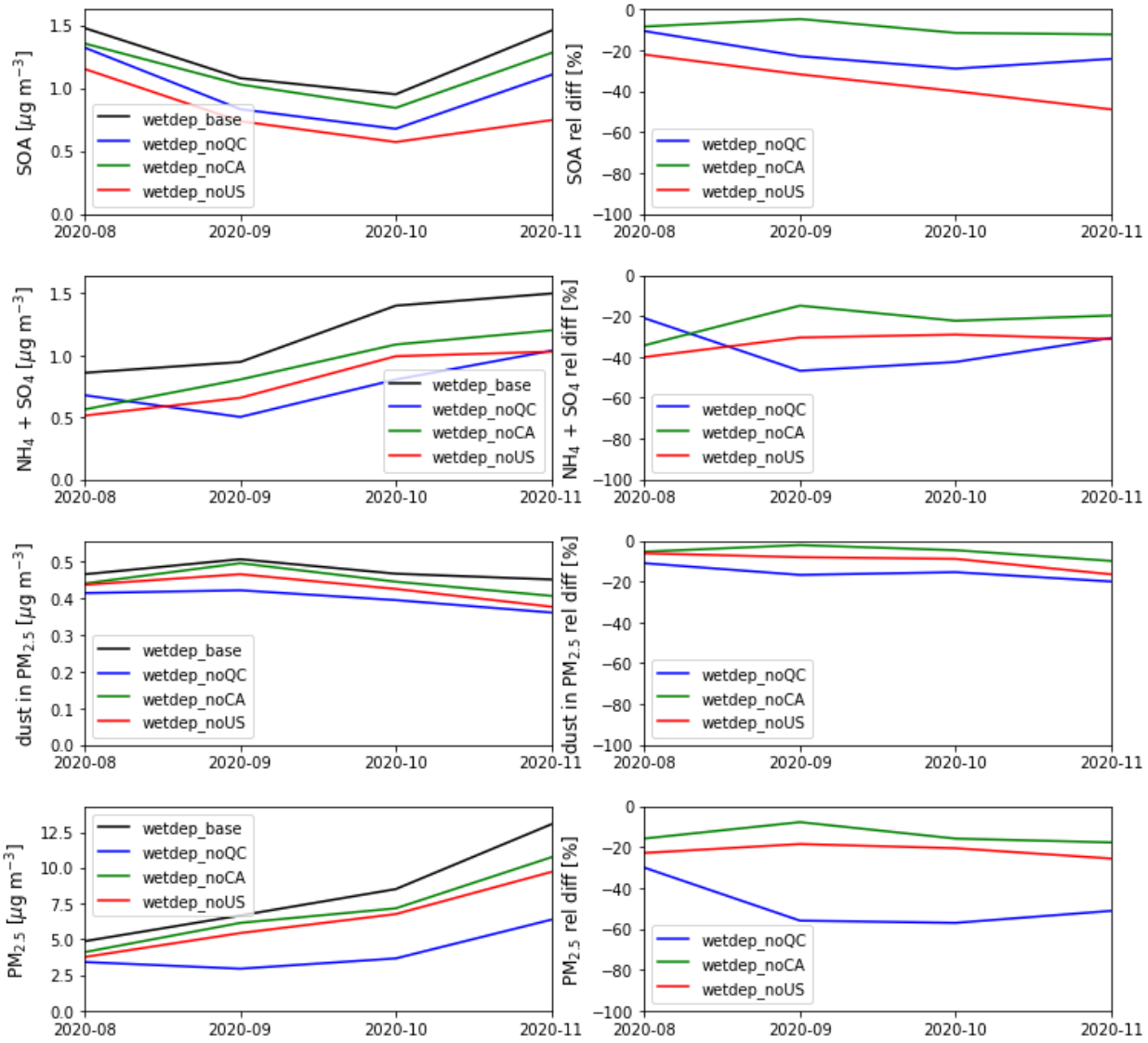

Fig. S4: GEOS-Chem simulations of (top) SOA, (middle 1) the sum of ammonium and sulfate concentrations, (middle 2) dust in $PM_{2.5}$, and (bottom) $PM_{2.5}$. The labels noQC, noCA, and noUS refer to simulations without anthropogenic emissions from Quebec, the rest of Canada, and the US, respectively.

Chemical mass closure

A chemical mass closure study was performed using the chemical composition measurements to estimate the contributions of the different components to the total $PM_{2.5}$ mass concentration following the method reported by Fakhri et al. (2023). Briefly, the contribution of sea salt is calculated by summing the six major ions (Sciare et al., 2005):

$$[\text{Sea salt}] = [Na^+] + [Cl^-] + [ss - Mg^{2+}] + [ss - K^+] + [ss - Ca^{2+}] + [ss - SO_4^{2-}] \quad \text{(Eq. 5)}$$

Ionic constituents such as K^+, Ca^{2+}, Mg^{2+} and SO_4^{2-} are derived from both marine and non-marine sources. Therefore, it is necessary to discriminate sea salt (ss) from non-sea salt (nss) contributions. Assuming that all sodium ions are of marine origin, the sea-salt contribution can be calculated based on sea water composition as shown in Eqs. 6 – 9 (Genga et al., 2017; Sciare et al., 2005). Furthermore, non-sea salt potassium, calcium, magnesium and sulfate (nss-K^+, nss-Ca^{2+}, nss-Mg^{2+} and nss-SO_4^{2-}) are calculated by subtracting the sea-salt fraction (ss-K^+, ss-Ca^{2+}, ss-Mg^{2+} and ss-SO_4^{2-}, respectively) from the total concentration of the ions (K^+, Ca^{2+}, Mg^{2+} and SO_4^{2-}, respectively).

$$[ss - SO_4^{2-}] = 0.252 \times [Na^+] \quad \text{(Eq. 6)}$$
$$[ss - Ca^{2+}] = 0.038 \times [Na^+] \quad \text{(Eq. 7)}$$
$$[ss - K^+] = 0.036 \times [Na^+] \quad \text{(Eq. 8)}$$
$$[ss - Mg^{2+}] = 0.119 \times [Na^+] \quad \text{(Eq. 9)}$$

In addition, secondary inorganic aerosol (SIA) is represented by the sum of nss-SO_4^{2-}, NH_4^+ and NO_3^-. To take bound water into account a hydration multiplication factor of 1.29 was applied to convert the dry inorganic concentrations (SIA and sea salt) into hydrated species (Sciare et al., 2005; Genga et al., 2017).

~~The contribution of crustal matter (CM) (Eq. 10) was estimated by summing the concentrations of aluminum, silicon, calcium, iron, and titanium in their oxide forms (Huang et al., 2014). The coefficients in front of the elements correspond to the additional mass due to oxygen in the minerals. Silicon was not measured in this study and was indirectly determined by multiplying the measured aluminum concentration by a factor of 3.41 (Esmaeilirad et al., 2020). This factor is obtained from the ratio of Si and Al in the Earth's crust following Mason and Moore (1982).~~

~~$[CM] = 2.2\,[Al] + 2.49\,[Si] + 1.63\,[Ca] + 2.42\,[Fe] + 1.94\,[Ti]$ (Eq. 10)~~

~~To find the optimal CF to calculate OM from OC, the factor was varied from 1.2 to 2.1. The Pearson correlation (R) calculated between the reconstructed $PM_{2.5}$ and the measured mass did not change significantly (0.978-0.979), but the highest correlation and the slope closest to 1 was obtained with CF=1.6. The results of chemical mass closure study are shown in Fig. S5.~~

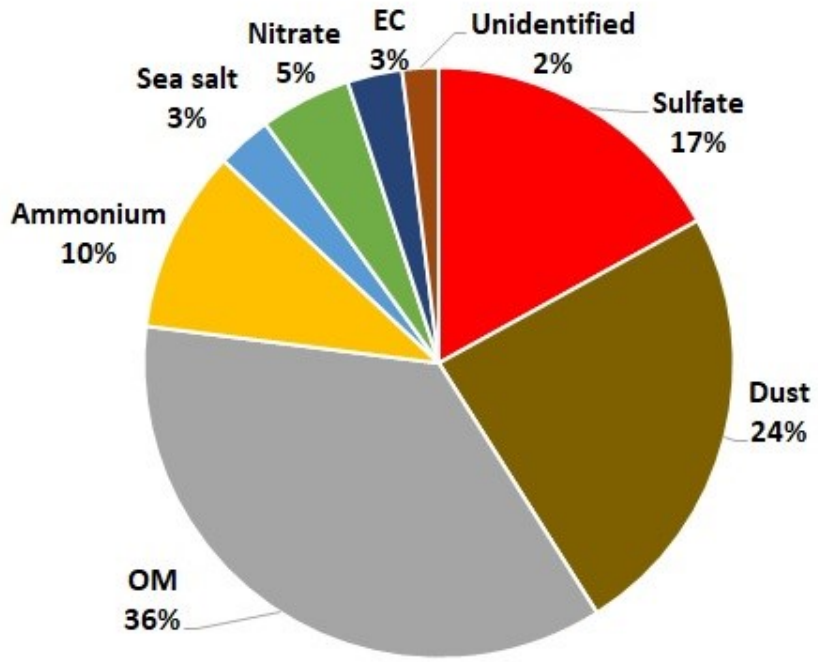

Fig. S5: Percent source contributions determined by chemical mass closure.

The indexes for the n-alkanes

Overall CPI and high CPI were calculated using the concentrations of n-alkanes following the Eq. 5~~11~~ and ~~12~~ 6 (Bray and Evans, 1961; Cooper and Bray, 1963; Fadel et al., 2021):

$$\text{Overall CPI} = \frac{\Sigma \text{ odd C15–C29}}{\Sigma \text{ even C16–C30}} \qquad \text{(Eq. ~~11~~5)}$$

$$\text{High CPI} = \frac{\Sigma \text{ odd C25–C29}}{\Sigma \text{ even C26–C30}} \qquad \text{(Eq. ~~12~~6)}$$

Biogenic sources emit larger amounts of odd carbon number alkanes than even carbon number alkanes, resulting in an Overall CPI greater than 6. Petrogenic emissions, on the other hand, have no carbon preference and have an Overall CPI value close to 1, whereas biomass burning has a value between 2 and 5 (Haque et al., 2019; Li et al., 2010; Fadel et al., 2021). When only the higher

molecular weight n-alkanes are considered, anthropogenic sources have CPI values below 1.5, while biogenic sources have CPI values higher than 3 (Caumo et al., 2020; Kang et al., 2020).

Furthermore, wax n-alkane concentrations were used to assess the relative contributions of biogenic and anthropogenic sources. The concentrations of wax n-alkanes (WNA), in the C14 to C30 range, and its percentage (%WNA) were calculated using the following equations (Fadel et al., 2021):

$$WNA_n = C_n - 0.5(C_{n-1} + C_{n+1}) \quad \text{(Eq. 137)}$$

$$\%WNA = \frac{\sum WNA}{\sum NA} \times 100 \quad \text{(Eq. 148)}$$

where C_n is the odd carbon congener, ΣWNA is the sum of wax n-alkane concentrations and ΣNA is the total concentration of n-alkanes. The %WNA value of 7.95±4.93% was indicative of smaller relative inputs from biogenic sources compared to the anthropogenic ones. Hence, the Overall CPI, High CPI and %WNA all appear to depict a similar picture of the anthropogenic origins of n-alkanes.

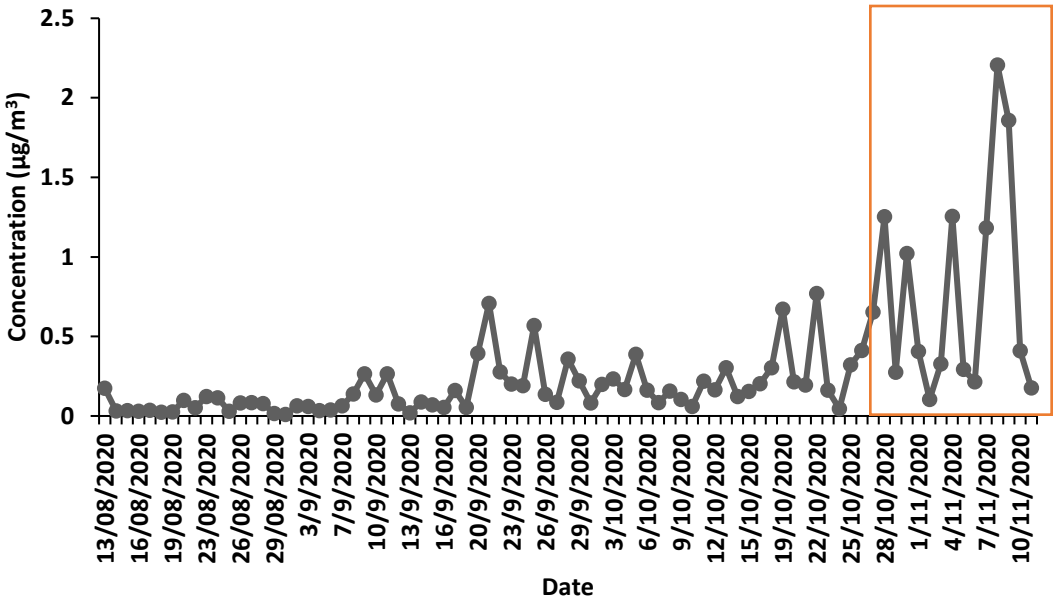

Fig. S6: The temporal variation of nitrate concentrations for the sampling period at MTL site.

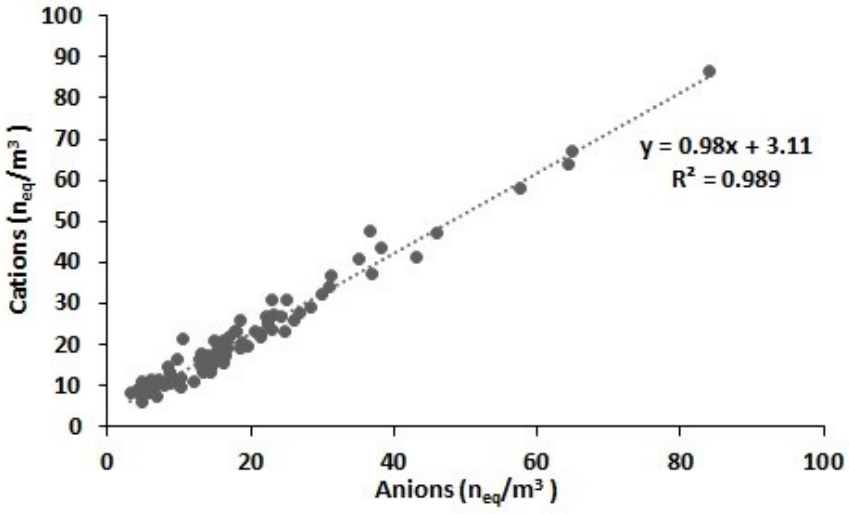

Fig. S7: Ion balance evaluation between the water-soluble ions (Cations: Na^+, Mg^{2+}, NH_4^+, K^+, Ca^{2+} and anions: SO_4^{2-}, NO_3^-, Cl^-).

Table S4: Species included in the PMF analysis.

Species	% of data below the DL	Species	% of data below the DL
OC	-	Levoglucosan	-
EC	-	7α[H]-21β[H]-Hopane	-
Na^+	-	Hexadecanoic acid	-
Cl^-	-	Octadecanoic acid	-
NH_4^+	-	C20	-
NO_3^-	-	C21	-
SO_4^{2-}	-	C24	-
Al	3	C25	-
Fe	1	C27	-
Ti	-	C29	-
Cu	4	Oxalic acid	-
Sb	3	Pinic acid	-
Cd	5	Cis-pinonic acid	-
Co	12		

Secondary organic carbon

While EC is derived only from combustion processes, organic carbon (OC) is produced by both primary and secondary sources. Several studies have estimated the contribution of secondary organic carbon (SOC) by employing the OC/EC minimum ratio method and the following equation (Castro et al., 1999; Shivani et al., 2019; Cesari et al., 2018; Calvo et al., 2008; Joseph et al., 2012).

$$SOC = OC_{total} - EC \times \left(\frac{OC}{EC}\right)_{min} \quad (Eq. 9)$$

In the first step, the OC/EC ratio is calculated for each sample, and $(OC/EC)_{min}$ is the minimum ratio observed in the samples. In this study, $(OC/EC)_{min}$ was 2.22. In the second step, the measured OC (OC_{total}) and EC for each sample are used with the minimum to calculate the SOC following the equation above.

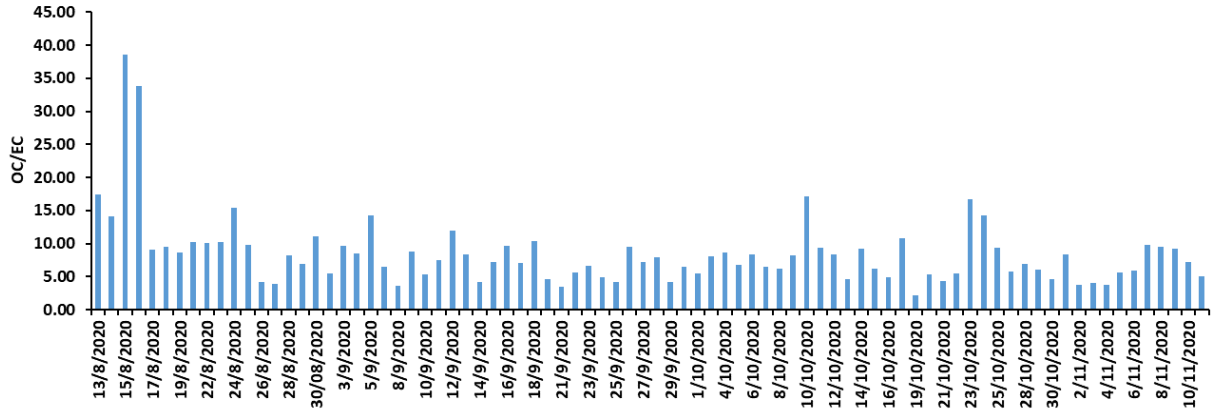

Fig. S9: The temporal variation of OC/EC ratio for the sampling period.

Pollution rose

The pollution roses in **Figure S10** displays the frequency of a given concentration of a factor as a function of wind direction. The wind data was taken from a nearby meteorological station at Montréal-Pierre Elliott Trudeau Airport. In general, the pollution rose plots are consistent with the identification of the factors proposed in the manuscript.

The traffic exhaust and road dust factors show similar polar plots with the highest concentrations of these factors being observed when the wind is from the southern and western directions. The observations of high factor concentrations with winds from these directions is expected given that major highways (Autoroutes 15 and 40) are located to the west and the south of the measurement

site, and winds from the south and west tend to have higher speeds facilitating transport. The road dust factor also exhibits some periods of very high concentrations when the wind is from the northeast, possibly due to the greater influence of very local emissions and surface streets.

In contrast, the biomass burning and crustal dust factors dust showed higher concentrations when winds were from the northeast. No major highways are in this direction. The biomass burning factor showed no trend with date during the campaign period. It is possible that this factor is related to certain food preparation activities such pizzerias and bagel bakeries that traditionally use wood ovens. Similarly, the crustal dust factor may be attributable to local construction activities, although further studies of the sources of these factors is needed. Interestingly, the cooking factor, unlike the biomass burning factor, shows little dependence on wind direction, which is reasonable given the measurement site is surrounded by residential neighborhoods and many restaurants.

The SIA and SOA factor both have similar dependences on wind direction with the highest concentrations tending to be observed when the wind is from the south and southwest. As already mentioned for the traffic-related factors above, winds from this direction can potentially transport aerosol and aerosol-precursors to the measurement site from major highways located to the south and southwest of the site. Alternatively, as discussed in the main text, GEOS-Chem modeling shows large transboundary contributions from the USA to these components. Thus, the wind blowing from the south may also correspond to large scale transport from south to north that increases the transboundary contribution to the SIA and SOA factors.

Both the biogenic SOA and plant wax factors exhibit high concentrations when winds are blowing from the northwest. In this direction is a major suburb of Montréal, Town of Mont-Royal, which contains a high density of trees relative to the rest of the metropolitan area. At the same time, we note that the biogenic SOA factor reaches moderately high concentrations for almost all wind

directions, suggesting the importance of regional formation, which is expected to be important for this factor.

The marine factor exhibits relatively high concentrations for multiple wind directions including from the west and southwest. Thus, the marine factor pollution rose resembles to some extent that of road dust. It is also notable that the marine factor exhibits its highest concentrations in November when minimum temperatures were below freezing, and some snowfall occurred. Thus, it is possible that is factor originates from road salt, although further work is needed to evaluate the contribution of road salt to $PM_{2.5}$ in Montréal.

Lastly, the industrial factor exhibits its highest concentration when winds are blowing from the west and north. Many major industries on the Island of Montreal are located to the northeast of the site (e.g., the Suncor Energy Refinery). Thus, the pollution rose for the industrial factor does not correspond to the location of these sources. This discrepancy may be explained by changes in wind direction upwind of the site, especially given that the distances to some of the largest potential emitters is approximately 10 km.

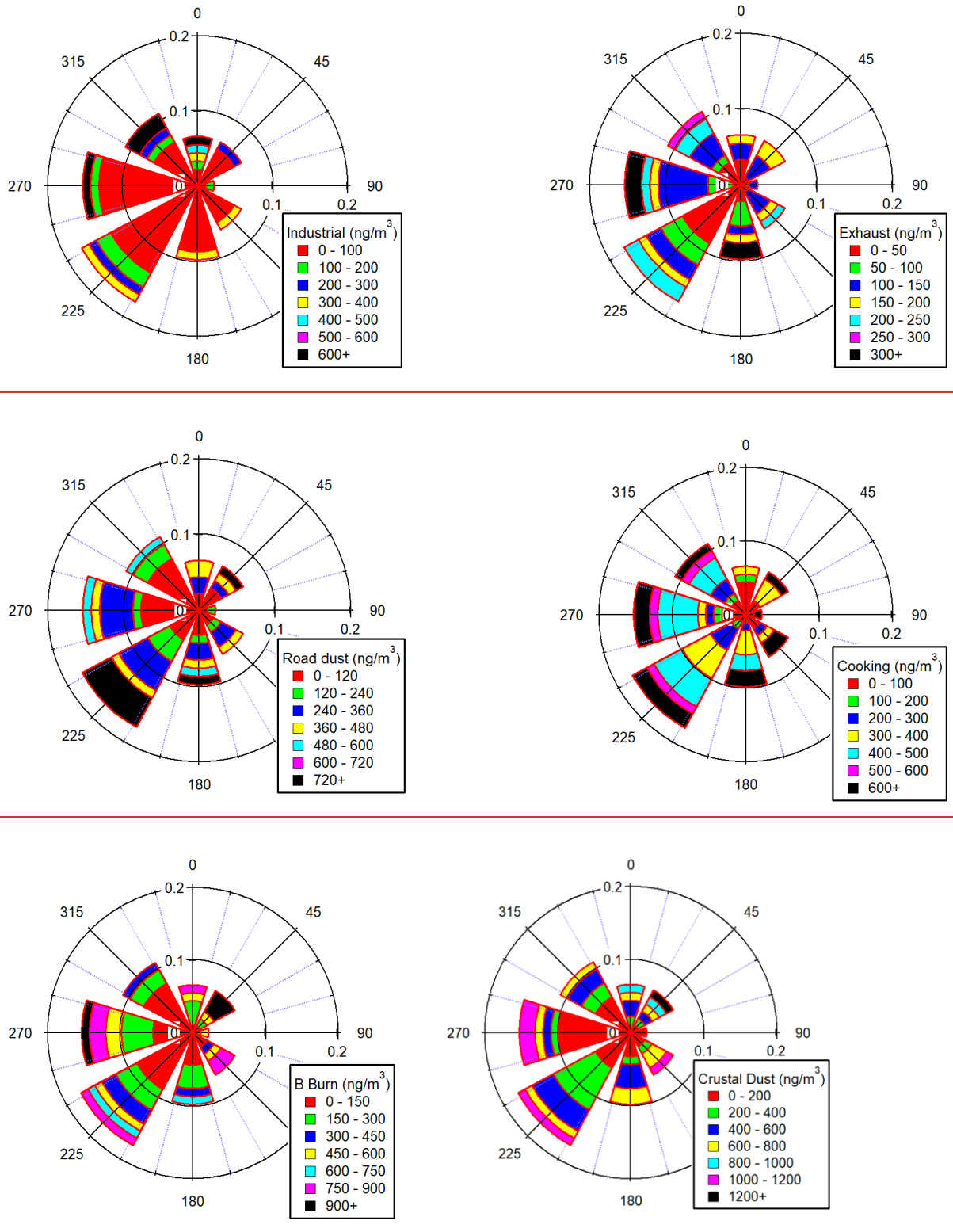

Fig. S10: Pollution rose plots for the PMF factors showing the frequency of a given concentration as function of wind direction.

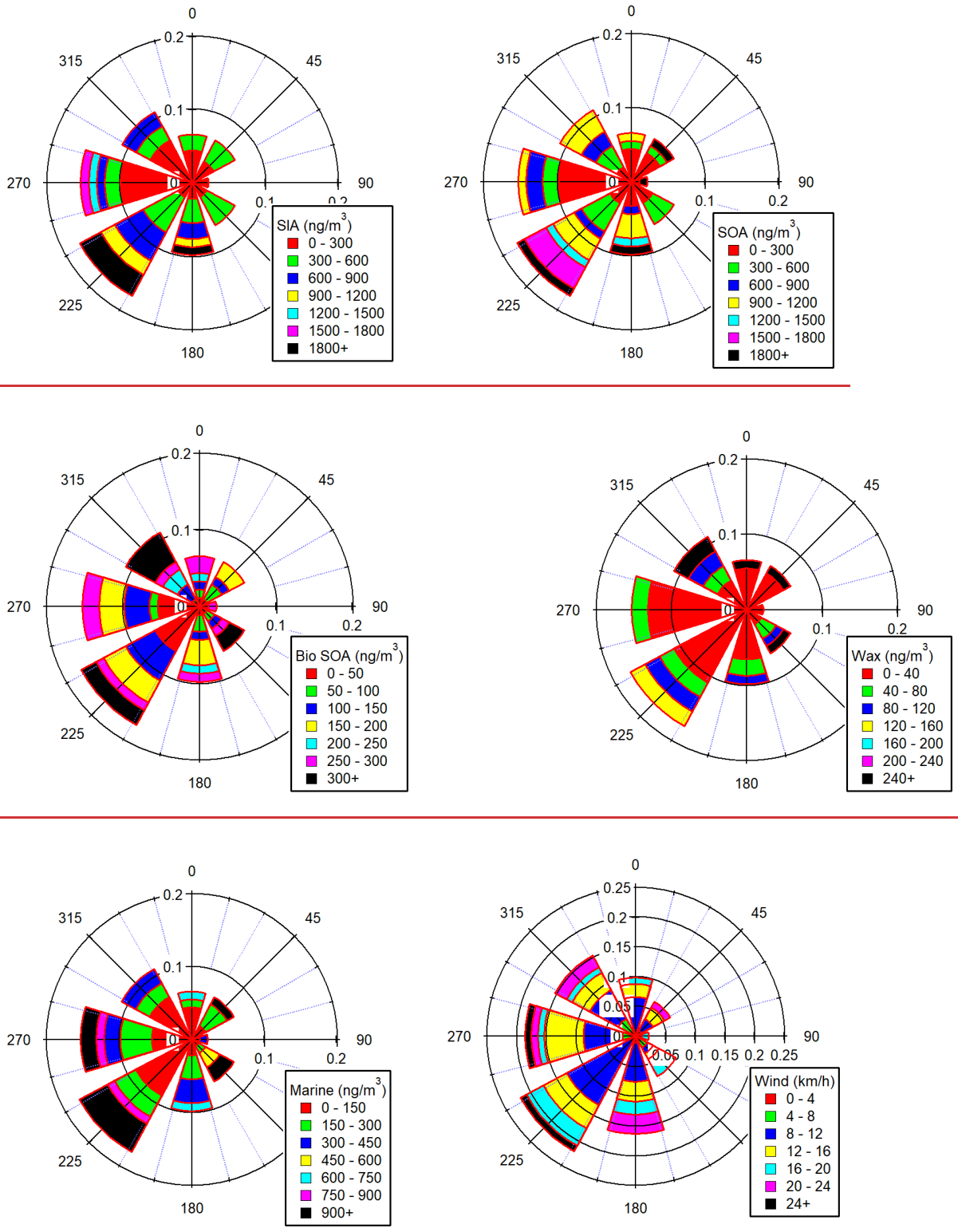

Fig. S10 (continued): Pollution rose plots for the PMF factors showing the frequency of a given concentration as function of wind direction.

References

Bray, E.E., Evans, E.D., 1961. Distribution of n-paraffins as a clue to recognition of source beds. Geochim. Cosmochim. Acta 22, 2–15. https://doi.org/10.1016/0016-7037(61)90069-2

Caumo, S., Bruns, R.E., Vasconcellos, P.C., 2020. Variation of the distribution of atmospheric n-alkanes emitted by different fuels' combustion. Atmos. 11, 1–19. https://doi.org/10.3390/atmos11060643

Calvo, A.I., Pont, V., Liousse, C., Dupré, B., Mariscal, A., Zouiten, C., Gardrat, E., Castera, P., Lacaux, C.G., Castro, A., Fraile, R., 2008. Chemical composition of urban aerosols in Toulouse, France during CAPITOUL experiment. Meteorol. Atmos. Phys. 102, 307–323. https://doi.org/10.1007/s00703-008-0319-2

Castro, L.M., Pio, C.A., Harrison, R.M., et al., 1999. Carbonaceous aerosol in urban and rural European atmospheres: estimation of secondary organic carbon concentrations. Atmos. Env. 33 (17), 2771-2781.

Cesari, D., De Benedetto, G.E., Bonasoni, P., Busetto, M., Dinoi, A., Merico, E., Chirizzi, D., Cristofanelli, P., Donateo, A., Grasso, F.M., Marinoni, A., Pennetta, A., Contini, D., 2018. Seasonal variability of $PM_{2.5}$ and PM_{10} composition and sources in an urban background site in Southern Italy. Sci. Total Environ. 612, 202–213. https://doi.org/10.1016/j.scitotenv.2017.08.230

Cooper, J.E., Bray, E.E., 1963. A postulated role of fatty acids in petroleum formation. Geochim Cosmochim. Acta 27, 1113–1127. doi:10. 1016/0016-7037(63)90093-0

Esmaeilirad, S., Lai, A., Abbaszade, G., Schnelle-Kreis, J., Zimmermann, R., Uzu, G., Daellenbach, K., Canonaco, F., Hassankhany, H., Arhami, M., Baltensperger, U., Prévôt, A.S.H., Schauer, J.J., Jaffrezo, J.L., Hosseini, V., El Haddad, I. 2020. Source apportionment of fine particulate matter in a Middle Eastern Metropolis, Tehran-Iran, using PMF with organic and inorganic markers. Sci. Total Environ. 705, 135330. https://doi.org/10.1016/j.scitotenv.2019.135330.

Fadel, Marc, Ledoux, F., Farhat, M., Kfoury, A., Courcot, D., Afif, C., 2021. $PM_{2.5}$ characterization of primary and secondary organic aerosols in two urban-industrial areas in the East Mediterranean. J. Environ. Sci. (China) 101, 98–116. https://doi.org/10.1016/j.jes.2020.07.030

Fakhri, N., Fadel, M., Öztürk, F., Keleş, M., Iakovides, M., Pikridas, M., Abdallah, C., Karam, C., Sciare, J., Hayes, P.L., Afif, C., 2023. Comprehensive chemical characterization of PM2.5 in the large East Mediterranean-Middle East city of Beirut, Lebanon. J. Environ. Sci. 133, 118–137. https://doi.org/10.1016/j.jes.2022.07.010

Genga, A., Ielpo, P., Siciliano, T., Siciliano, M., 2017. Carbonaceous particles and aerosol mass closure in $PM_{2.5}$ collected in a port city. Atmos. Res. 183, 245–254.

Haque, M.M., Kawamura, K., Deshmukh, D.K., Fang, C., Song, W., Mengying, B., Zhang, Y.L., 2019. Characterization of organic aerosols from a Chinese megacity during winter: Predominance of fossil fuel combustion. Atmos. Chem. Phys. 19, 5147–5164. https://doi.org/10.5194/acp-19-5147-2019

Huang, X.H.H., Bian, Q., Ng, W.M., Louie, P.K.K., Yu, J.Z., 2014. Characterization of $PM_{2.5}$ major components and source investigation in suburban Hong Kong: A one year monitoring study. Aerosol Air Qual. Res. 14, 237–250.

Joseph, A.E., Unnikrishnan, S., Kumar, R., 2012. Chemical characterization and mass closure of fine aerosol for different land use patterns in Mumbai city. Aerosol Air Qual. Res. 12, 61–72. https://doi.org/10.4209/aaqr.2011.04.0049

Kang, M., Kim, K., Choi, N., Kim, Y.P., Lee, J.Y., 2020. Recent occurrence of PAHs and n-Alkanes in pm2.5 in Seoul, Korea and characteristics of their sources and toxicity. Int. J. Environ. Res. Public Health 17. https://doi.org/10.3390/ijerph17041397

Lee, E., Chan, C.K., Paatero, P., 1999. Application of positive matrix factorization in source apportionment of particulate pollutants in Hong Kong. Atmos. Environ. 33, 3201–3212. https://doi.org/10.1016/S1352-2310(99)00113-2

Li, W., Peng, Y., Bai, Z., 2010. Distributions and sources of n-alkanes in $PM_{2.5}$ at urban, industrial and coastal sites in Tianjin, China. J. Environ. Sci. 22, 1551–1557. https://doi.org/10.1016/S1001-0742(09)60288-6

Mason, B., Moore, C.B., 1982. Principles of Geochemistry, fourth edition. Wiley.

Meng, J., Martin, R. V., Li, C., van Donkelaar, A., Tzompa-Sosa, Z. A., Yue, X., Xu, J.-W., Weagle, C. L., and Burnett, R. T.: Source Contributions to Ambient Fine Particulate Matter for Canada, Environ. Sci. Technol., 53, 10269–10278, https://doi.org/10.1021/acs.est.9b02461, 2019.

Sciare, J., Oikonomou, K., Cachier, H., Mihalopoulos, N., Andreae, M.O., Maenhaut, W., et al., 2005. Aerosol mass closure and reconstruction of the light scattering coefficient over the Eastern Mediterranean Sea during the MINOS campaign. Atmos. Chem. Phys. Discuss. 5, 2427–2461.

Schutgens, N. A. J., Gryspeerdt, E., Weigum, N., Tsyro, S., Goto, D., Schulz, M., and Stier, P.: Will a perfect model agree with perfect observations? The impact of spatial sampling, Atmos. Chem. Phys., 16, 6335–6353, https://doi.org/10.5194/acp-16-6335-2016, 2016.

Shivani, Gadi, R., Sharma, S.K., Mandal, T.K., 2019. Seasonal variation, source apportionment and source attributed health risk of fine carbonaceous aerosols over National Capital Region, India. Chemosphere 237, 124500. https://doi.org/10.1016/j.chemosphere.2019.124500